THE JOURNAL OF PHYSICAL CHEMISTRY B

Article

pubs.acs.org/JPCB

Calibration of 1,2,4-Triazole-3-Thione, an Original Zn-Binding Group of Metallo-β-Lactamase Inhibitors. Validation of a Polarizable MM/MD Potential by Quantum Chemistry

Karolina Kwapien,[†,‡] Mirna Damergi,[§,∥] Serge Nader,[†,∥] Léa El Khoury,[§,∥] Zeina Hobaika,[∥] Richard G. Maroun,[∥] Jean-Philip Piquemal,[§,⊥,#] Laurent Gavara,[¶] Dorothée Berthomieu,[‡] Jean-François Hernandez,[¶] and Nohad Gresh*[,§]

[†]Chemistry and Biology, Nucléo(s)tides and Immunology for Therapy (CBNIT), UMR 8601, CNRS, UFR Biomédicale, Paris, France

[‡]Institut Charles-Gerhardt, MACS, UMR 5253 CNRS-ENSCM-UM, 8 rue de l'Ecole Normale, 34296 Montpellier Cedex 5, France

[§]Laboratoire de Chimie Théorique, Sorbonne Universités, UPMC, UMR7616 CNRS, Paris, France

[∥]Centre d'Analyses et de Recherche, UR EGFEM, LSIM, Faculté des Sciences, Saint Joseph University of Beirut, BP 11-514, Riad El Solh, Beirut 1116-2050, Lebanon

[⊥]Institut Universitaire de France, Paris Cedex 05, 75231, France

[#]Department of Biomedical Engineering, The University of Texas at Austin, Austin, Texas 78712, United States

[¶]Institut des Biomolécules Max Mousseron, UMR 5247 CNRS, Faculté de Pharmacie, Université de Montpellier, ENSCM, 15 avenue Charles Flahault, 34093 Montpellier, France

Supporting Information

ABSTRACT: In the context of the SIBFA polarizable molecular mechanics/dynamics (PMM/PMD) procedure, we report the calibration and a series of validation tests for the 1,2,4-triazole-3-thione (TZT) heterocycle. TZT acts as the chelating group of inhibitors of dizinc metallo-β-lactamases (MBL), an emerging class of Zn-dependent bacterial enzymes, which by cleaving the β-lactam bond of most β-lactam antibiotics are responsible for the acquired resistance of bacteria to these drugs. Such a study is indispensable prior to performing PMD simulations of complexes of TZT-based inhibitors with MBL's, on account of the anchoring role of TZT in the dizinc MBL recognition site. Calibration was done by comparisons to energy decomposition analyses (EDA) of high-level *ab initio* QC computations of the TZT complexes with two probes: Zn(II), representative of "soft" dications, and water, representative of dipolar molecules. We performed distance variations of the approach of each probe to each of the two TZT atoms involved in Zn ligation, the S atom and the N atom *ortho* to it, so that each SIBFA contribution matches its QC counterpart. Validations were obtained by performing in- and out-of-plane angular variations of Zn(II) binding in monoligated Zn(II)−TZT complexes. The most demanding part of this study was then addressed. How well does ΔE(SIBFA) and its individual contributions compare to their QC counterparts in the dizinc binding site of one MBL, L1, whose structure is known from high-resolution X-ray crystallography? Six distinct complexes were considered, namely each separate monozinc site, and the dizinc site, whether ligated or unligated by TZT. Despite the large magnitude of the interaction energies, in all six complexes ΔE(SIBFA) can match ΔE(QC) with relative errors <2% and the proper balance of individual energy contributions. The computations were extended to the dizinc site of another MBL, VIM-2, and its complexes with two other TZT analogues. ΔE(SIBFA) faithfully reproduced ΔE(QC) in terms of magnitude, ranking of the three ligands, and trends of the separate energy contributions. A preliminary extension to correlated calculations is finally presented. All these validations should enable a secure design of a diversity of TZT-containing MBL inhibitors: a structurally and energetically correct anchoring of TZT should enable all other inhibitor groups to in turn optimize their interactions with the other target MBL residues.

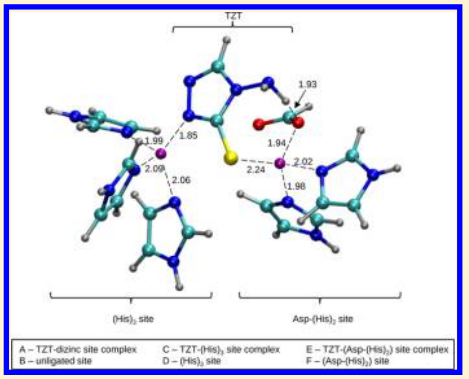

INTRODUCTION

Metallo-β-lactamases (MBL) are an important class of bacterial mono- and dizinc-dependent metalloenzymes, which are responsible for the inactivating cleavage of most β-lactam antibiotics and are mainly produced by Gram-negative bacteria responsible for nosocomial diseases.[1,2] They are a major cause of acquired resistance to these antibiotics and represent a major health threat worldwide.[3,4] Whereas inhibitors of other β-lactamases classes with a catalytic serine are available as marketed drugs, yet there presently exists no MBL inhibitor

Received: February 2, 2017
Revised: June 2, 2017
Published: June 2, 2017

DOI: 10.1021/acs.jpcb.7b01053
J. Phys. Chem. B 2017, 121, 6295−6312

with sufficient affinity and specificity to be used clinically. On a brighter tone, several MBL's have lent themselves to high-resolution X-ray crystallography, in both the absence and the presence of an inhibitor. This is the case for L1,[5,6] VIM-2,[7] and NDM-1,[8] the latter two being currently disseminating in important opportunistic Gram-negative pathogens.[9,10] The availability of such structures should enable for docking and drug-design studies. But which accuracy could be expected for docking regarding the intermolecular interaction energies with the dizinc core, owing to the onset of very large polarization, charge-transfer, and nonadditivity effects, which have been unraveled by quantum chemistry?[11,12]

The present work is part of a multidisciplinary approach, which integrates chemical synthesis, biochemical and microcalorimetry evaluations, X-ray structural analyses and computational chemistry of novel MBL inhibitors. These inhibitors contain the 1,2,4-triazole-3-thione (TZT, Figure 1a–c) heterocycle as a

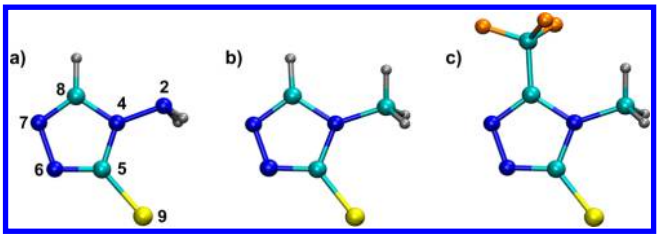

Figure 1. Model system of (a) TZT ring with the numbering of atoms used in the calculations and two other TZT derivatives: (b) TZT–CH_3 and (c) TZT–CH_3–CF_3 (N, blue; C, cyan; S, yellow; H, gray; F, orange).

Zn-binding motif. TZT bears a net negative charge, delocalized over its conjugated five-membered ring and the extracyclic S atom, S9. Initially proposed by Olsen et al.[13] for L1 inhibition based on an *in silico* study, the first X-ray structure (PDB-2HB9) of a TZT-containing compound complexed to a dizinc MBL (i.e., L1 from *Stenotrophomonas maltophilia*) was resolved by the group of Dideberg.[6] This structure revealed an unprecedented binding mode as the TZT motif was simultaneously coordinating the two zinc cations of L1 catalytic site through its sulfur and its nitrogen at position 6 (see Figure 1 and Figure 2). Since then, several papers reported the use of this scaffold in MBL inhibition.[14–16] Such structural information should enable to evolve, upon resorting to computational chemistry, the available TZT-based inhibitors into derivatives with further enhanced MBL affinities. Toward this aim, accounting correctly for the structural and energetic aspects of TZT binding to such Zn-binding sites is a prerequisite to MM/MD simulations of TZT-based inhibitor–dizinc MBL complexes. The presence of two Zn cations and the highly polarizable character of all Zn-binding ligands result in the onset of very strong electrostatic, polarization, and charge-transfer effects. In addition, several "promiscuous" interligand interactions take place, such as between the partly acidic CH proton of one His residue and the π electron cloud of a neighboring His: a correct representation of the short-range repulsion, not only in-plane, but also over the rings, is mandatory.

Ab initio QC calculations enable highly accurate intermolecular interaction energies, ΔE, but cannot be used routinely for complexes of several thousands of atoms, such as MBL's and their solvating waters. Several examples have shown the SIBFA polarizable MM/MD procedure[17] to reproduce closely ΔE(QC) in a diversity of complexes of inhibitors with the recognition site of metalloproteins[18–20] including the MBL of *Bacteroides fragilis*[21,22] and kinases,[23] totaling up to 265 atoms and 45 interacting molecules. This validates the use of SIBFA for the entirety of the MBL complexes, toward extending the realm of QC to complexes of several thousands of atoms.

In this context, the first step was to calibrate the TZT motif and to calculate the complex formed with the dizinc active site of the MBL L1 based on the experimental structure PDB-2HB9.[6] TZT is a challenging Zn-binding motif. In the MBL

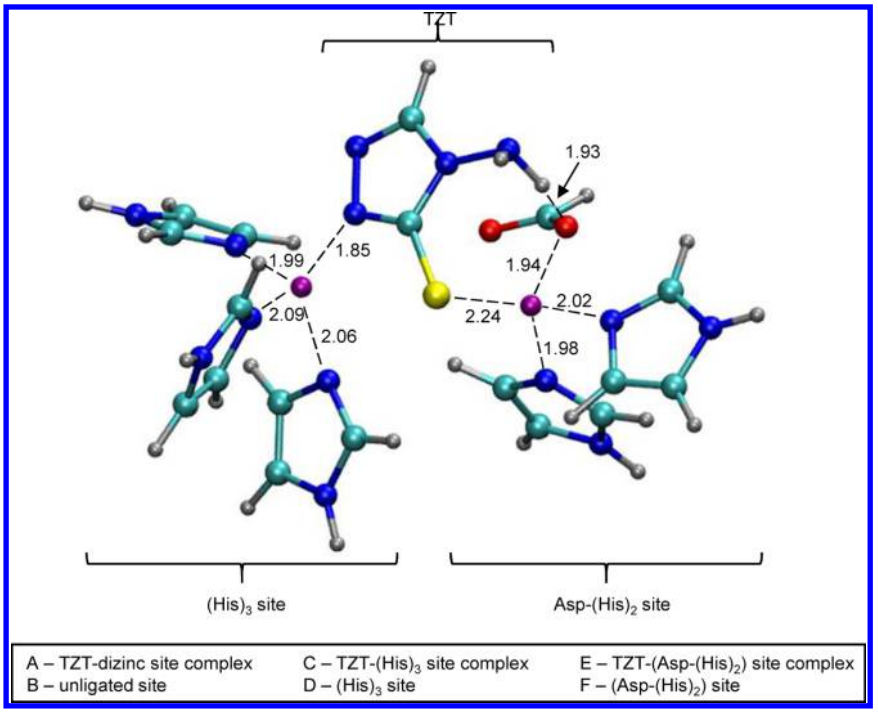

Figure 2. Active site of L1 protein with TZT ring (N, blue; C, cyan; S, yellow; H, gray; Zn^{2+}, purple; O, red). The relevant distances are given in Å.

DOI: 10.1021/acs.jpcb.7b01053
J. Phys. Chem. B 2017, 121, 6295–6312

active site, it bears an anionic charge delocalized over its extra-cyclic S atom and its pentacyclic ring, which embodies three N atoms. In the compound complexed to L1 in PDB-2HB9, the nitrogen at position 6 (see Figure 1 for numbering of the atoms and Figure 2 for binding mode) binds to Zn1, which is coordinated by three His side-chains (His_3 Zn-binding site) while the extra-cyclic sulfur atom binds to Zn2, which is coordinated by one Asp and two His side-chains (Asp-His_2 Zn binding site). In addition, the N at position 4 is substituted with an extracyclic amine, which acts as a proton donor to the Zn2-binding Asp side-chain. It is noteworthy that a similar binding was recently reported for another TZT compound with a methyl substituent at position 4 in the dizinc catalytic site of VIM-2.[24]

The present investigation was carried in four steps. We first performed QC energy decomposition analyses (EDA) for the approach of a Zn(II) or of a water probe to the S9 and N6 atoms (see atom numbering on Figure 1). For Zn(II), we investigated radial variations for in-plane binding, as well as for the perpendicular approach to the ring. At equilibrium distance, we performed in-plane variation of the θ angle (Zn−S−C or Zn−N−C) followed by out-of-plane variations at a fixed θ angle.

The different ways of Zn(II) approaching the TZT are presented in Figures 3a−3d and 4a−4d. For the water probe, only in-plane angular variation was studied.

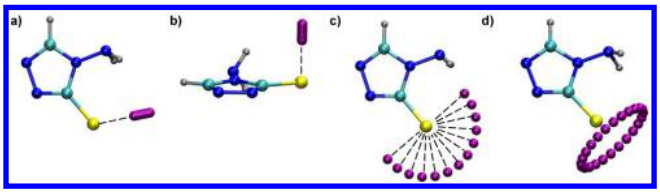

Figure 3. Probing of S−Zn(II) interaction by Zn(II) approaching S9 (a) along, (b) over, (c) in plane, and (d) out of plane (N, blue; C, cyan; S, yellow; H, gray; Zn(II), purple).

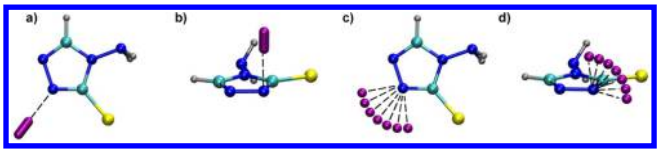

Figure 4. Probing of N−Zn(II) interaction by Zn(II) approaching N6 (a) along, (b) over, (c) in plane, and (d) out of plane (N, blue; C, cyan; S, yellow; H, gray; Zn(II), purple).

Calibration of the relevant TZT parameters was done so that each SIBFA contribution could reproduce the radial (in-plane and perpendicular) behavior of its QC counterpart: electrostatic, short-range repulsion, polarization, charge-transfer and dispersion. This was followed by validation of the in- and out-of-plane angular variations.

In the second step, we considered six complexes: the complete dizinc site with and without TZT (denoted as *A* and *B*), and similarly the separated Asp-His_2 and His_3 sites with and without ligand (denoted as *C*−*F*, see Figure 2). This enabled us to compare the SIBFA values to their QC counterparts, taking into account the evolution of each energy contribution upon when passing from *A* to *F*.

In the third step, we evaluated the transferability of the TZT-derived parameters to two other substituted derivatives. The first has a methyl substituent replacing the amino one. The second has, in addition, an electron-withdrawing substituent, trifluoromethane, *ortho* to the CH_3 group. These two derivatives are represented in Figure 1, parts b and c. We compare the intermolecular interaction energies of the three derivatives in another MBL recognition site, that of VIM-2. As for L1, both the dizinc binding site and both monozinc sites were considered. We addressed an essential issue in the design of novel derivatives of a given Zn-binding motif: can the QC-derived distributed mutipoles and polarizabilities used in SIBFA enable this procedure to quantify the impact on electron distribution brought about by electron withdrawing or electron-donating substituents?

Finally, in the fourth step, we performed a preliminary extension to correlated computations. A prior recalibration of TZT was done on the basis of SAPT calculations of its S9- and N6-bound complexes with one Zn(II) cation or with one water molecule. We then recomputed the intermolecular interaction energies in the L1 dizinc site and in the two monozinc sites as well as their complexes at the B97-D3 level. To these we compared the SIBFA results, now with correlated multipoles and polarizabilities.

PROCEDURE

Quantum-Chemistry (QC) Calculations. The QC calculations resorted to the aug-cc-pVTZ(-f) and the cc-pVTZ(-f) basis sets.[25,26] The latter was used whenever the complexes were not amenable to aug-cc-pVTZ(-f) calculations because of their sizes. Energy decomposition analyses (EDA) resorted to the RVS analysis due to Stevens and Fink[27] and coded in the GAMESS-US package.[28] The basis set superposition error (BSSE) was computed by the Boys and Bernardi procedure.[29] Calculations at the correlated level resorted to the B97-D3 energy functional augmented with the dispersion correction by Grimme et al.[30] The DFT calculations were done with the G09 package.[31] Energy-decomposition at the correlated levels were done using the symmetry-adapted perturbation procedure (SAPT) at the DFT level[32] with the Psi-4 package[33] and the ALMOEDA procedure[34] using the QChem package.[35]

SIBFA Calculations. In the SIBFA procedure[17] the intermolecular interaction energy is computed as the sum of five contributions: electrostatic multipolar (E_{MTP*}), short-range repulsion (E_{rep}), polarization (E_{pol}), charge transfer (E_{ct}), and dispersion (E_{disp})

$$\Delta E_{TOT} = E_{MTP*} + E_{rep} + E_{pol} + E_{ct} + E_{disp}$$

E_{MTP*} is computed with distributed multipoles (up to quadrupoles) derived from the QC molecular orbitals precomputed for each individual molecule using the generalized multipole analysis (GDMA) method by Stone.[36,37] It is augmented with a penetration term.[38,39] The anisotropic polarizabilities intervening in the expression of E_{pol} are distributed on the centroids of the localized orbitals (heteroatom lone pairs and bond barycenters) using a procedure due to Garmer and Stevens.[40] E_{rep} and E_{ct}, the two short-range repulsions, are computed using representations of the molecular orbitals localized on the chemical bonds and on localized lone-pairs.[39,41] E_{disp} is computed as an expansion into $1/R^6$, $1/R^8$, and $1/R^{10}$, and also embodies an explicit exchange-dispersion term.[42]

The distributed polarizabilities at the correlated level were derived with an in-home version[66] of the Hondo code.[43]

We will denote throughout this paper by E_1 the sum of the two first-order contributions, E_C and E_X in QC and E_{MTP*} and

DOI: 10.1021/acs.jpcb.7b01053
J. Phys. Chem. B 2017, 121, 6295−6312

Table 1. Interaction Energies (in kcal/mol) for In-Plane Binding of Zn(II) to S9, as a Function of Distance,[a] at a Fixed θ Angle of 120°

	E_C/E_{MTP*}		E_X/E_{REP}		E_{CX}/E_1		E_{POL}		E_{CT}		E_2		E_{TOTAL}	
dist [Å]	RVS	SIBFA	RVS	SIBFA	RVS	SIBFA	RVS	SIBFA	RVS	SIBFA	RVS	SIBFA	RVS	SIBFA
1.8	−322.6	−327.0	208.8	225.3	−113.9	−101.7	−116.8	−128.3	−53.5	−57.3	−170.3	−185.5	−298.9	−287.3
1.9	−300.6	−298.1	153.3	149.6	−147.3	−148.5	−111.0	−117.9	−48.5	−52.0	−159.5	−169.9	−318.1	−318.4
2.0	−281.1	−274.1	112.8	100.4	−168.3	−173.7	−106.0	−107.9	−45.1	−47.6	−151.0	−155.5	−328.3	−329.2
2.1	−264.1	−254.1	83.3	68.0	−180.7	−186.1	−101.6	−98.4	−42.8	−44.0	−144.4	−142.4	−332.4	−328.5
2.2	−249.0	−237.2	61.8	46.4	−187.2	−190.7	−97.9	−89.3	−41.4	−41.4	−139.3	−130.7	−332.6	−321.5
2.3	−235.7	−222.7	46.0	31.9	−189.7	−190.8	−94.5	−80.9	−40.7	−39.9	−135.2	−120.8	−330.2	−311.6
2.4	−223.8	−210.2	34.4	22.1	−189.5	−188.2	−91.6	−73.0	−40.6	−39.8	−132.2	−112.9	−326.3	−301.0
2.5	−213.2	−199.4	25.8	15.4	−187.4	−184.0	−89.0	−65.8	−41.0	−42.1	−130.0	−107.9	−321.6	−291.9

[a]Equilibrium distance =2.2 Å.

E_{rep} in SIBFA, and by E_2 the sum of the two second-order contributions, E_{pol} and E_{ct}.

Calibration. The calibration of TZT was performed as follows.

Electrostatic Contributions, E_{MTP} and E_{pol}. No recalibration was done for the penetration component of E_{MTP*}, the effective radii of N and S atoms being those calibrated recently for imidazole N and thiolate S atoms. The multiplicative factor and the exponent of the Gaussian function, which screens the polarizing field[44] were fit so as to match the radial behavior of E_{pol}(RVS) upon varying the Zn−S distance at an angle θ (C−S−Zn) of 120°. The best agreement was found for 0.48 and 1.80, respectively.

Short-Range Contributions, E_{rep} and E_{ct}. The S-relevant parameters were calibrated upon varying the Zn−S distance, the C−S−Zn angle being set at 120°. This enabled to fit E_{rep} and E_{ct} by comparisons to E_X(RVS) and E_{ct}(RVS), respectively, upon modifying the increments of the S effective radii used for these contributions along the direction of the six sp^3 S lone pairs, each of which having an occupation number of one. The other S parameters are those recently calibrated for the methane-thiolate ligand.[45] The parameters for the Zn-ligating N atom were fit upon varying the Zn−N distance along the external bisector of the nitrogen atom. This again enabled to fit E_{rep} and E_{ct} upon modifying the increment of the N effective radius along the sp lone-pair, both for its in-plane component, and for each of its two "smeared" components on both sides of the TZT plane. The occupation numbers of the in-plane and smeared sp components, and the distance of the smeared component from the N bearer were the same as those previously fit for the Zn-binding nitrogen of imidazole. The increments of the effective radii of the ring C and N atoms along the directions of their π lone-pairs were fit so that E_{rep} and E_{ct} match the radial evolutions of E_X(RVS) and E_{ct}(RVS), respectively, upon varying the distance of the probe Zn(II) binding to the ring atom along the perpendicular to the ring. In the Supporting Information, we give the locations of the lone-pairs in internal coordinates, their occupation numbers, and the increments of effective radii of their bearer along the lone pair direction (see Table S1). A figure with the lone-pair centroids as fictitious atoms is also given (see Figure S1).

RESULTS AND DISCUSSION

1. Monoligated Complexes. Probing the Thiolate Sulfur (S9) and N6 of TZT. TZT owing to its anionic nature is represented without protonated N atoms in the cycle. The extracyclic N atom on the other hand bears two protons and has an sp^3 hybridization. Energy-minimization of TZT starting from an sp^2 hybridization on this atom with two in-plane H atoms brought back the sp^3 form as is represented on Figure 1. Parts a−d of Figure 3 represent the Zn-positions explored upon probing the thiolate sulfur S9. Figure 3a corresponds to radial in-plane variations at the fixed θ (C−S−Zn) angle of 120°, *trans* from N6, and Figure 3b corresponds to radial variations perpendicular to the plane; Figure 3c corresponds to in-plane 15° stepwise variations of θ at the optimized S−Zn distance of 2.2 Å and Figure 3d corresponds to out-of-plane 15° stepwise variations of the ϕ (N6−C5−S9—Zn) angle at the fixed S−Zn distance of 2.2 Å and fixed θ angle of 120°.

Similarly, parts a and b of Figure 4 represent the Zn-positions explored for in- and out-of-plane radial variations of the N6−Zn distance, namely, for Figure 4a, in-plane along the external bisector of N6 and for Figure 4b, along the perpendicular to the plane passing through N6. For the optimized N6−Zn distance, parts c and d of Figure 4 represent respectively the in-plane variations of θ (C5−N6−Zn) angle around the external bisector, and the out-of-plane variations of ϕ (N4−C5−N6-Zn) angle starting from the in-plane, external bisector position until the perpendicular position is reached.

The radial dependencies of ΔE(SIBFA) and ΔE(QC) and their contributions are compared in Tables 1−4. The corresponding graphical representations are given in Supporting Information Figures S2 and S3 regarding binding to sulfur S9 and S5 and S6 regarding binding to nitrogen N6. The in- and out-of-plane angular variations are presented on Figures 5 and 6 for sulfur S9 and Figures 7 and 8 for nitrogen N6 with the corresponding values listed in Tables S2, S3, S5, and S6. In addition, Figures S4 and S7 together with Tables S4 and S7 display the θ-energy dependencies for the binding of another probe, water, donating a proton to sulfur S9 and nitrogen N6 respectively.

Radial Variations of Zn(II) and HOH. Table 1 shows that in the range of distances 1.9—2.2 Å ΔE(SIBFA) retains a close agreement with ΔE(QC), with relative errors <3%. There is a very close agreement of E_1(SIBFA) with E_1(RVS) from 1.9 Å throughout, although it results from compensations between underestimations of E_C and EX by their SIBFA counterparts. The lesser agreement of ΔE values occurring past 2.2 Å is mainly due to E_{pol} decaying much faster in SIBFA than in RVS. The reason for such faster decays remains unclear. These should be of limited impact, however, owing to the reduction of the magnitude of E_{pol} in polyligated complexes due to anticooperativity. Indeed, much closer agreement between E_{pol}(SIBFA) and E_{pol}(QC) in several polyligated complexes was previously

DOI: 10.1021/acs.jpcb.7b01053
J. Phys. Chem. B 2017, 121, 6295−6312

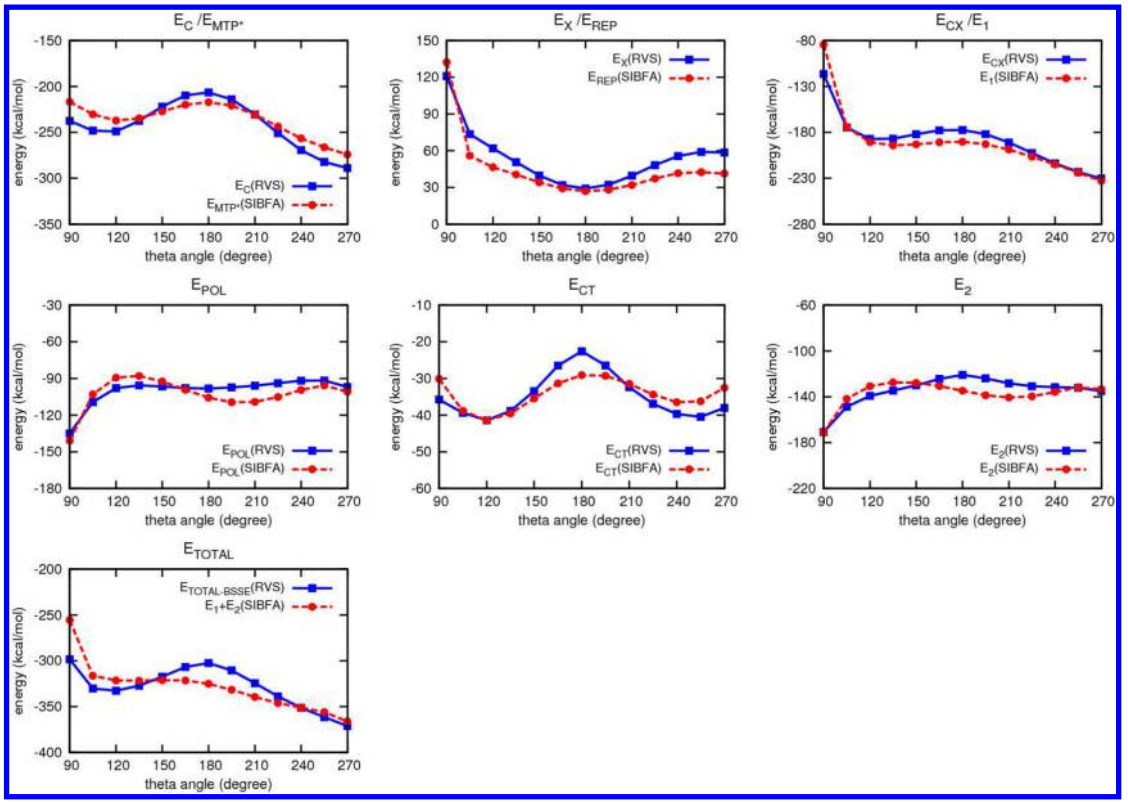

Figure 5. Zn(II) in plane of S9. Comparison between QM and SIBFA total interaction energies and their contributions as a function of θ angle (d = 2.20 Å).

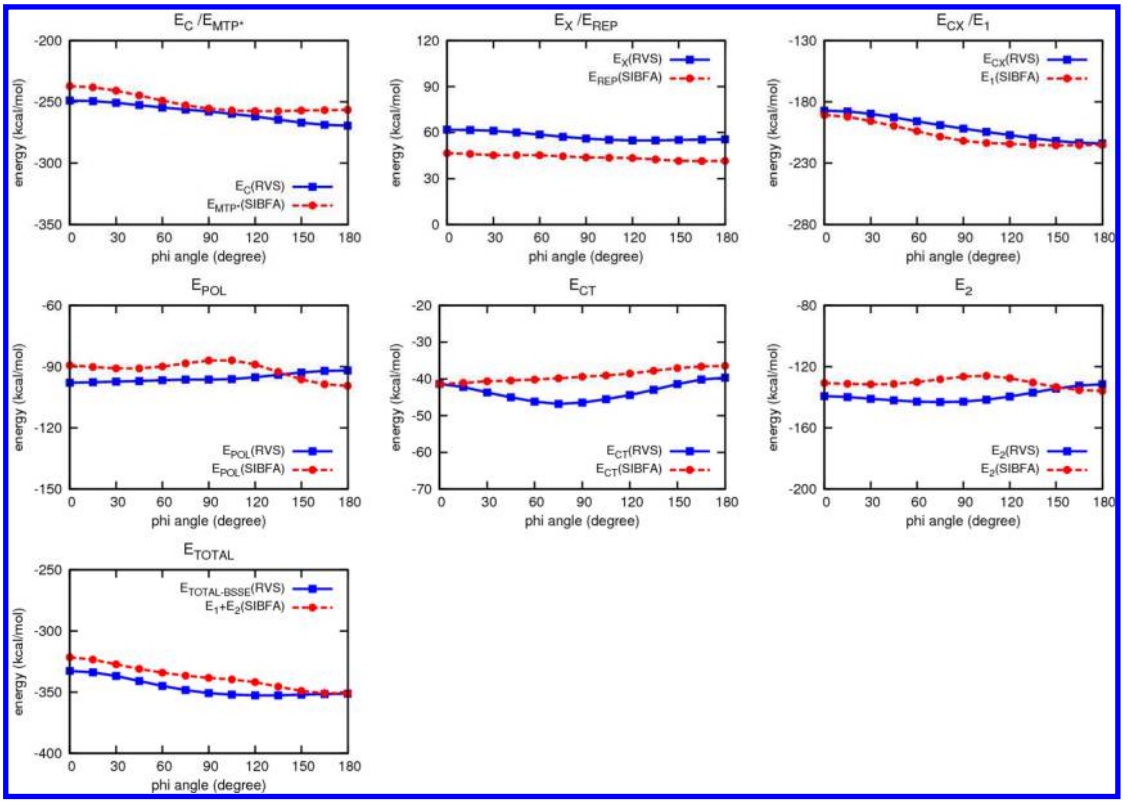

Figure 6. Zn(II) out of plane of S9. Comparison between QM and SIBFA total interaction energies and their contributions as a function of ϕ angle (d = 2.20 Å, θ = 120°).

noted and will also be shown in this paper as well. E_{ct} has a very slow decay past 2.1 Å, becoming shallow past 2.2 Å. As noted earlier,[44,46] this can be ascribed to a state interchange with a state having a neutral TZT and monocationic Zn. Again, this

DOI: 10.1021/acs.jpcb.7b01053
J. Phys. Chem. B 2017, 121, 6295−6312

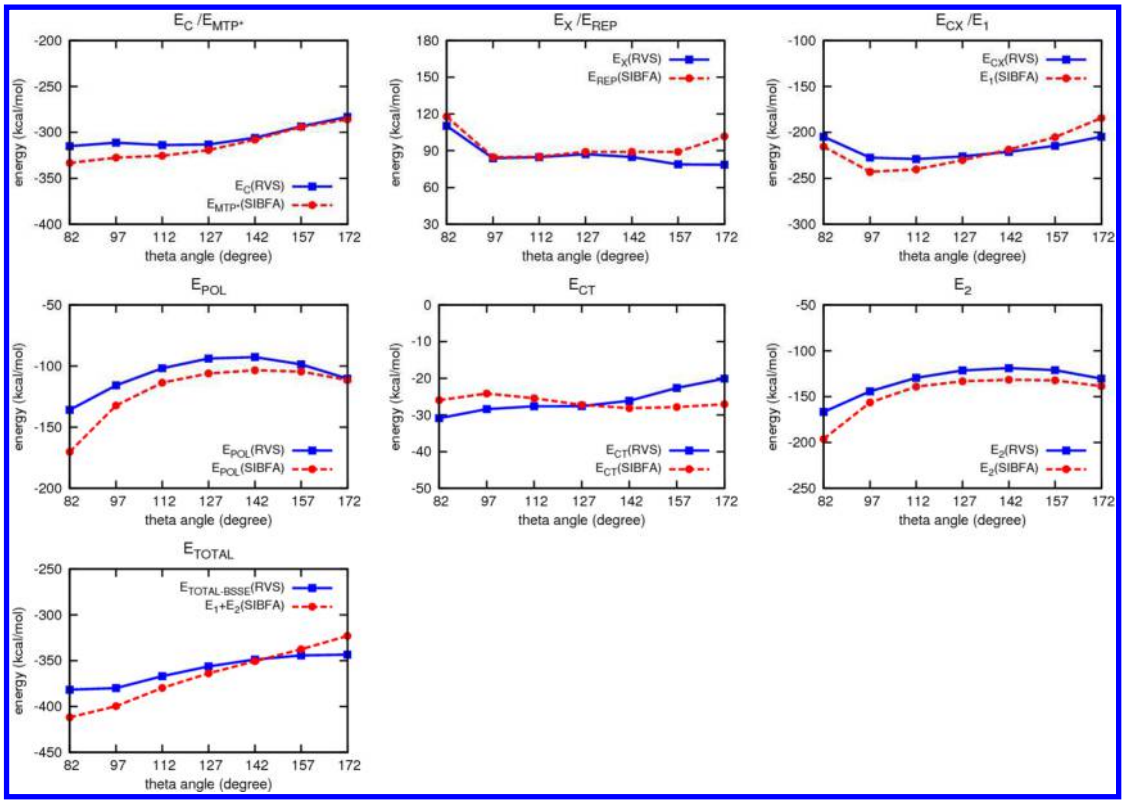

Figure 7. Zn(II) in plane of N6. Comparison between QM and SIBFA total interaction energies and their contributions as a function of θ angle (d = 1.80 Å).

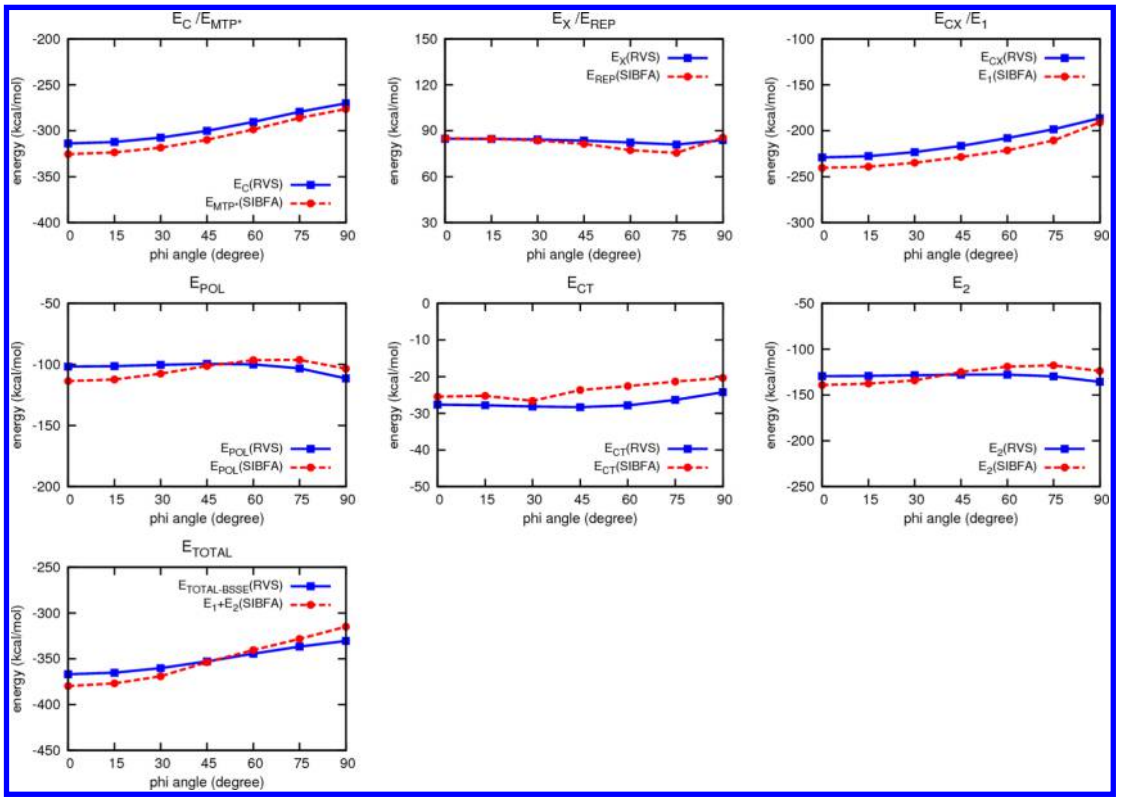

Figure 8. Zn(II) out of plane of N6. Comparison between QM and SIBFA total interaction energies and their contributions as a function of ϕ angle (d = 1.80 Å, θ = 112°).

should not impair the agreement in polyligated complexes, where such state interchanges are prevented by the additional Zn-ligands. Table 2 shows good agreements are limited to a range of distances 1.9 Å − 2.2 Å, past which ΔE(SIBFA) becomes smaller in magnitude than ΔE(RVS): this is again, mostly due to the faster decrease of E_{pol}(SIBFA) than E_{pol}(RVS).

DOI: 10.1021/acs.jpcb.7b01053
J. Phys. Chem. B 2017, 121, 6295−6312

Table 2. Interaction Energies (in kcal/mol) for Perpendicular Binding of Zn(II) to S9, as a Function of Distance[a]

	E_C/E_{MTP*}		E_X/E_{REP}		E_{CX}/E_1		E_{POL}		E_{CT}		E_2		E_{TOTAL}	
dist [Å]	RVS	SIBFA	RVS	SIBFA	RVS	SIBFA	RVS	SIBFA	RVS	SIBFA	RVS	SIBFA	RVS	SIBFA
1.8	−336.3	−343.9	210.6	192.9	−125.7	−151.0	−118.1	−124.6	−54.7	−51.7	−172.8	−176.3	−313.6	−327.3
1.9	−315.6	−316.2	154.5	130.9	−161.1	−185.3	−112.1	−114.2	−50.0	−46.8	−162.1	−161.0	−334.7	−346.3
2.0	−297.3	−293.2	113.6	89.3	−183.7	−203.9	−106.8	−104.2	−47.0	−42.6	−153.8	−146.8	−346.6	−350.8
2.1	−281.2	−273.9	83.7	61.2	−197.5	−212.7	−102.2	−94.9	−45.2	−39.2	−147.4	−134.0	−352.3	−346.7
2.2	−267.0	−257.5	61.9	42.2	−205.1	−215.3	−98.1	−86.0	−44.4	−36.4	−142.5	−122.5	−353.9	−337.8
2.3	−254.4	−243.3	46.0	29.1	−208.4	−214.2	−94.5	−77.8	−44.4	−34.6	−139.0	−112.4	−352.8	−326.6
2.4	−243.2	−231.1	34.3	20.2	−208.9	−210.9	−91.4	−70.2	−45.2	−33.7	−136.5	−103.9	−350.2	−314.7
2.5	−233.1	−220.3	25.6	14.1	−207.5	−206.2	−88.5	−63.1	−46.5	−34.3	−135.0	−97.4	−346.7	−303.7

[a]Equilibrium distance = 2.2 Å.

Table 3. Interaction Energies (in kcal/mol) for In-Plane Binding of Zn(II) to N6, as a Function of Distance[a]

	E_C/E_{MTP*}		E_X/E_{REP}		E_{CX}/E_1		E_{POL}		E_{CT}		E_2		E_{TOTAL}	
dist [Å]	RVS	SIBFA	RVS	SIBFA	RVS	SIBFA	RVS	SIBFA	RVS	SIBFA	RVS	SIBFA	RVS	SIBFA
1.8	−313.3	−319.5	87.0	89.0	−226.3	−230.5	−93.8	−106.0	−27.6	−27.2	−121.4	−133.3	−356.3	−363.7
1.9	−294.4	−297.5	60.3	58.8	−234.2	−238.8	−88.1	−94.5	−26.0	−23.2	−114.1	−117.7	−355.0	−356.5
2.0	−278.5	−278.9	41.9	39.2	−236.6	−239.8	−83.2	−84.1	−24.7	−20.4	−107.9	−104.5	−350.0	−344.2
2.1	−264.8	−263.0	29.2	26.3	−235.7	−236.7	−79.0	−74.8	−23.8	−17.1	−102.7	−91.9	−342.8	−328.6
2.2	−252.9	−249.1	20.3	17.7	−232.6	−231.4	−75.1	−66.5	−23.3	−12.4	−98.4	−78.9	−334.7	−310.3
2.3	−242.5	−237.1	14.2	12.1	−228.3	−225.0	−71.4	−59.1	−23.5	−10.2	−94.9	−69.4	−326.3	−294.4
2.4	−233.1	−226.5	9.9	8.2	−223.3	−218.2	−67.7	−52.6	−24.5	−8.4	−92.2	−61.0	−318.1	−279.2
2.5	−224.7	−217.0	6.9	5.6	−217.9	−211.4	−64.1	−46.8	−26.3	−7.0	−90.4	−53.7	−310.5	−265.1

[a]Equilibrium distance = 1.8 Å.

Table 4. Interaction Energies (in kcal/mol) for Perpendicular Binding of Zn(II) to N6, as a Function of Distance[a]

	E_C/E_{MTP*}		E_X/E_{REP}		E_{CX}/E_1		E_{POL}		E_{CT}		E_2		E_{TOTAL}	
dist [Å]	RVS	SIBFA	RVS	SIBFA	RVS	SIBFA	RVS	SIBFA	RVS	SIBFA	RVS	SIBFA	RVS	SIBFA
1.8	−262.8	−261.6	89.5	89.5	−173.3	−172.1	−114.6	−122.3	−22.3	−18.1	−136.9	−140.3	−318.1	−312.4
1.9	−249.5	−248.1	62.0	63.2	−187.5	−184.9	−106.4	−108.2	−20.6	−16.4	−126.9	−124.6	−320.6	−309.5
2.0	−238.5	−236.2	43.0	44.7	−195.5	−191.5	−99.0	−95.7	−19.1	−15.4	−118.1	−111.1	−318.5	−302.6
2.1	−229.1	−225.7	29.9	31.7	−199.2	−194.0	−92.1	−84.7	−18.0	−14.1	−110.2	−98.8	−314.6	−292.8
2.2	−220.9	−216.4	20.7	22.5	−200.2	−193.9	−85.7	−75.0	−17.9	−9.9	−103.6	−84.9	−306.6	−278.8
2.3	−213.7	−208.1	14.4	16.0	−199.3	−192.1	−79.6	−66.4	−19.3	−8.6	−99.0	−75.0	−300.4	−267.1
2.4	−207.2	−200.7	9.9	11.4	−197.3	−189.2	−73.9	−58.9	−22.5	−7.5	−96.4	−66.4	−295.5	−255.6
2.5	−201.4	−193.9	6.9	8.2	−194.5	−185.8	−68.4	−52.4	−27.4	−6.5	−95.8	−58.9	−282.0	−244.6

[a]Equilibrium distance = 1.9 Å.

Contrary to the S-bound complexes, the in-plane binding is significantly favored over the perpendicular one for the N6-bound complexes (Tables 3 and 4). At equilibrium distance, all SIBFA energy contributions match the QC ones. The agreement becomes lesser upon increasing the Zn−N distance, owing to the faster decay of both E_{pol} and E_{ct}(SIBFA) as compared to their QC counterparts.

In- and Out-of Plane Zn(II)- and HOH-Binding to S9. Figure 5 and Table S2 report the in-plane evolutions of ΔE and their contributions as a function of θ. The best agreements, with relative errors <2% are in the 225−270° range, which also corresponds to the lowest-energy range. In this range, there are also close agreements in the E_1 and E_2 values. The least agreements, in the range 90−120° and 165−210° ranges, concern ΔE values that are 39−73 kcal/mol less stabilizing.

Figure 6 and Table S3 report the out-of-plane evolutions of ΔE and their contributions. Here again, the closest agreements, with relative errors of 2%, are for the most stable complexes, in the 135−180° range of ϕ values. In this range, there is a close, uniform match of E_1 and E_2(SIBFA) with their QC counterparts, but, again, with some compensations of errors between SIBFA and QC electrostatic and short-range repulsion within E_1, and polarization and charge-transfer within E_2. Table S4 reports the in-plane TZT−water intermolecular interaction energies for water approaching S9 through on H atom upon θ variations at a fixed S9−H(OH) distance of 2.3 Å, the angle S9−H−O being 180°.

In- and Out-of Plane Zn(II)- and HOH-Binding to N6. Figure 7 and Table S5 report the results for in-plane variations of the θ angle. The most favorable θ value is 82°, for which Zn(II) can bridge N6 and S9. Such a binding mode is, however, unlikely to occur in the MBL binding site, in which N6 and S9 each bind to a distinct Zn(II) cation. There is a unusually large overestimation of ΔE(RVS) by ΔE(SIBFA), amounting to 8%, caused mainly by E_{pol}. This unusual overestimation of E_{pol} might indicate the limitations of the Gaussian screening function used in SIBFA, when a dipositive cation closely bridges two heteroatoms belonging to a conjugated ligand. More advanced screening functions are presently implemented, and it will be highly instructive to evaluate their

DOI: 10.1021/acs.jpcb.7b01053
J. Phys. Chem. B 2017, 121, 6295−6312

Table 5. Interaction Energies (in kcal/mol) for L1 Dizinc Site with and without Ligand (TZT)

	TZT−dizinc site complex (A)			unligated site (B)		
	RVS			RVS		
energy contribution RVS/SIBFA	cc[a]	augcc[b]	SIBFA	cc	augcc	SIBFA
E_C/E_{MTP*}	−1060.8		−1094.6	−622.6		−643.3
E_X/E_{REP}	400.8		401.5	241.3		248.2
E_{CX}/E_1	−660.1		−693.2	−381.4		−395.1
E_{POL}	−314.4		−332.7	−313.3		−331.7
$E_{POL(VAR)}$	−241.2		−242.0	−242.8		−263.0
E_{CT}	−100.0			−100.3		
$E_{CT\text{-}BSSE}$	−90.8		−70.4	−94.2		−59.7
E_2	−332.1		−314.6	−337.0		−322.7
$\Delta E_{RVS}/\Delta E_{SIBFA}$[c]	**−992.1**		**−1007.8**	**−718.4**		**−717.8**
ΔE_{HF}	**−1001.3**	**−991.0**		**−724.5**	**−717.6**	

[a]cc: cc-pVTZ(-f) basis set. [b]augcc: augcc-pVTZ(-f) basis set. [c]ΔE_{RVS} includes the BSSE correction

Table 6. Interaction Energies (kcal/mol) for $(His)_3$ Site in L1 with and without Ligand (TZT)

	TZT−$(His)_3$ site complex (C)			$(His)_3$ site (D)		
	RVS			RVS		
energy contribution RVS/SIBFA	cc[a]	augcc[b]	SIBFA	cc	augcc	SIBFA
E_C/E_{MTP*}	−535.1	−538.3	−553.0	−263.7	−266.7	−270.2
E_X/E_{REP}	192.4	204.2	200.1	110.5	116.5	114.2
E_{CX}/E_1	−342.7	−334.0	−352.9	−153.3	−150.1	−156.0
E_{POL}	−160.2	−174.1	−169.7	−149.5	−160.4	−153.5
$E_{POL(VAR)}$	−123.7	−134.7	−126.9	−120.4	−130.3	−126.3
E_{CT}	−46.6	−40.2		−43.3	−35.1	
$E_{CT\text{-}BSSE}$	−43.2	−38.7	−32.7	−42.6	−34.3	−29.2
E_2	−166.9	−173.4	−159.6	−161.9	−164.5	−155.4
$\Delta E_{RVS}/\Delta E_{SIBFA}$[c]	**−509.5**	**−507.4**	**−512.5**	**−315.2**	**−314.6**	**−311.4**
ΔE_{HF}	**−512.9**	**−508.9**		**−316.9**	**−315.5**	

[a]cc: cc-pVTZ(-f) basis set. [b]augcc: augcc-pVTZ(-f) basis set. [c]ΔE_{RVS} includes the BSSE correction.

performances in such cases. The trends upon varying θ are reflected by SIBFA, except for E_{ct}, which is more regular in SIBFA than in RVS.

Figure 8 and Table S6 report the evolutions for out-of-plane binding to N6. There are closer agreements between SIBFA and QC, the relative errors being always <3.5% and the trends of E_1 and E_2 and their individual contributions being more consistent than for in-plane binding. It is noted that contrary to S-binding, the preferential position is in-plane, while for S-binding, a perpendicular position of approach is preferred. Water was chosen as another TZT probe owing to the following: (a) there are TZT−MBL complexes in which two water molecules remain TZT-bound in the recognition site;[24] (b) TZT−water complexes need to be accurately computed since TZT solvation is to be included in the energy balances for MBL complexation; (c) water is of interest as a representative of dipolar molecules, and it is important to evaluate how these can be "sensed" by TZT. Table S7 reports the in-plane TZT−water intermolecular interaction energies for water approaching N6 through one H atom upon θ variations at a fixed N6−H(OH) distance of 1.9 Å, the angle N6−H−O being 180°.

The present tests are demanding as they are carried out at equilibrium distances. In polyligated complexes, the Zn-ligand distances can increase due to the sharing of the Zn(II) cation by four up to five or six ligands, and the second-order terms should diminish in magnitude due to anticooperativity. Such factors should result into an improved agreement between SIBFA and QC. This will be addressed next, upon considering the polyligated arrangements of one and two Zn(II) cations in TZT-ligated and unligated MBL binding site.

2. Polyligated Complexes. Having completed the calibration and validation of TZT, we now address the critical part of this investigation. In the perspective of docking simulations of TZT-containing inhibitors, which accuracy could be expected from SIBFA regarding TZT binding to the dizinc recognition site? We present in Figure 2 the X-ray crystal structure of MBL L1 dizinc binding site bound to the TZT moiety of the inhibitor 4-Amino-2,4-dihydro-5-(2-methylphenyl)-3*H*-1,2,4-triazole-3-thione named IIIA (PDB-2HB9).[6] It shows N6 ligating one Zn(II) cation (Zn1) in the His_3 binding site, and S9 ligating the second Zn(II) cation (Zn2) in the Asp-His_2 binding site. Figure 2 shows also the most relevant interatomic distances. The Zn1−N6 and Zn2−S9 distances of 1.85 and 2.24 Å, respectively, are close to those optimized in the monoligated complexes. Zn−His and Zn−Asp distances are "standard" Zn distances to the MBL imidazole N atoms in the range 1.85−2.10 Å and to one Asp side-chain O atom of 1.95 Å. There is also an additional interaction (with a distance of 1.93 Å) between the Zn-coordinating O of Asp and one H atom of the extracyclic NH_2 substituent. But in addition we can note several interligand distances between partly acidic H atoms belonging to CH bonds *ortho* to a Zn-ligating N atom on one imidazole, and either the Zn-ligating N atom or a C atom *ortho* to it, belonging to a neighboring imidazole, whether on the same or on the other MBL Zn-binding site. Such distances are illustrated in Supporting Information Figure S8.

DOI: 10.1021/acs.jpcb.7b01053
J. Phys. Chem. B 2017, 121, 6295−6312

Table 7. Interaction Energies (kcal/mol) for (Asp-His$_2$) Site in L1 with and without Ligand (TZT)

	TZT−(Asp-(His)$_2$) site complex (E)			(Asp-(His)$_2$) site (F)		
	RVS			RVS		
energy contribution RVS/SIBFA	cc[a]	augcc[b]	SIBFA	cc	augcc	SIBFA
E_C/E_{MTP*}	−641.4	−647.8	−646.4	−474.5	−478.1	−477.9
E_X/E_{REP}	205.6	225.7	197.3	126.3	137.2	130.0
E_{CX}/E_1	−435.7	−422.1	−449.1	−348.2	−340.8	−347.9
E_{POL}	−133.5	−152.0	−136.4	−113.1	−126.4	−120.7
$E_{POL(VAR)}$	−105.7	−118.8	−101.7	−96.2	−106.6	−100.1
E_{CT}	−52.9	−45.2		−42.6	−34.2	
$E_{CT\text{-}BSSE}$	−47.5	−43.8	−36.8	−39.0	−33.4	−29.9
E_2	−153.2	−162.7	−138.5	−135.2	−140.0	−130.0
$\Delta E_{RVS}/\Delta E_{SIBFA}$[c]	**−588.9**	**−584.7**	**−587.6**	**−483.4**	**−480.8**	**−477.9**
ΔE_{HF}	**−594.3**	**−586.1**		**−487.1**	**−481.6**	

[a]cc: cc-pVTZ(-f) basis set. [b]augcc: augcc-pVTZ(-f) basis set. [c]ΔE_{RVS} includes the BSSE correction

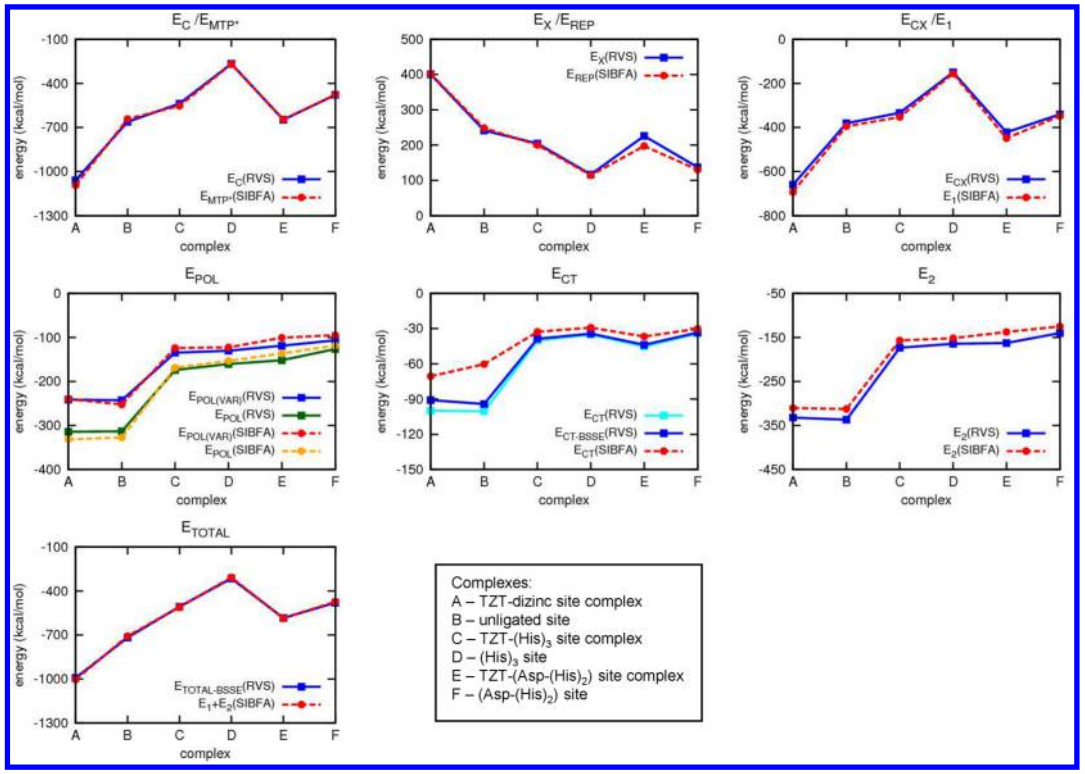

Figure 9. L1 with TZT ring. Comparison between QM and SIBFA total interaction energies and their contributions in different Zn(II) binding sites.

These interactions take place over the electron-rich ring of the approached imidazole. Their onset stresses the need for a correct representation of not only electrostatic effects regarding E_{MTP} and E_{pol} but also of short-range effects regarding E_{rep} and E_{ct}: the latter feature reemphasizes the need for a proper handling of π and smeared σ lone-pairs, as addressed in this work and a previous paper.[45]

Table 5 gives the values of ΔE(QC) and ΔE(SIBFA) and their contributions in the complete dizinc complex with (A) and without (B) TZT ligand. This enables to evaluate the impact of TZT binding on the quality of the SIBFA results as compared to the QC ones. The SIBFA versus QC comparisons are also carried out for the two individual Zn(II) binding sites, and are reported in Tables 6 and 7. Such additional tests can be very important: to trace back the origin of shortcomings of SIBFA, if any, found in the dizinc site to ΔE imbalances occurring in one or both monozinc sites; or, alternatively, to ensure that a satisfactory reproduction of the QC results, if it indeed occurred in the dizinc site, does preexist in both monozinc sites as well. The RVS analyses are carried out with the aug-cc-pVTZ(-f) and cc-pVTZ(-f) basis sets, except for the two dizinc complexes for which, due to size limitations, the RVS analyses could be only done at the cc-pVTZ(-f) level. Nevertheless the values of ΔE(QC)/aug-cc-pVTZ(-f) (without RVS analysis) are very close to the cc-pVTZ(-f) ones.

Table 5 shows a very close agreement of ΔE(SIBFA) and ΔE(QC) in the TZT−dizinc complex, with a very small relative error of 1.5%. There are, however, some error compensations. For the TZT-ligated complex, some overestimation of E_C by E_{MTP*} is compensated by a concomitant underestimation of E_{ct}. A very close agreement between ΔE(SIBFA) and ΔE(QC) is also found in the unligated complex, with a relative error of 1.5%. The same compensations of errors are seen as in the TZT-ligated complex, namely some overestimation of E_C by

DOI: 10.1021/acs.jpcb.7b01053
J. Phys. Chem. B 2017, 121, 6295−6312

E_{MTP*} compensated by an underestimation of E_{ct}. On the other hand, E_{rep} and E_{pol} can closely match their QC counterparts, E_X and E_{pol}, in both cases. Alternatives to GDMA to derive the distributed E_{MTP*} multipoles will be discussed below. They should enable to improve the agreement between E_{MTP*} and E_C: thus, complexes such as those of L1 and VIM-2 recognition sites will further serve as benchmarks for such alternative procedures. The reasons for the underestimation of E_{ct}(SIBFA) remain to be elucidated. Its expression embodies dependencies upon the multipolar potentials and fields undergone by the electron donor and the electron acceptor.[44] Investigating the impact of an improved E_{MTP*} representation on E_{ct} will be the incentive of a future study.

There are very close agreements between SIBFA and QC results regarding the His_3 site, with relative errors of 2% (see Table 6). Here also the error compensations concern E_{MTP*} which overestimates E_C, although by much smaller amounts than in the dizinc site, and E_{ct}, which is underestimated by SIBFA, although, here again, much less significantly than in the dizinc site. It is noted that E_{rep}(SIBFA) and E_{pol}(SIBFA) again have close values to the QC ones, both of them having values intermediate between the aug-cc-pVTZ(-f) and cc-pVTZ(-f) ones.

Close SIBFA/QC agreements are also found for the $Asp(His)_2$ site, the relative errors not exceeding 2% (see Table 7). There is a more uniform agreement in terms of individual contributions. Whether in the unligated or TZT-ligated site, no particular QC contribution seems to be misrepresented by SIBFA, except possibly E_{ct} in the TZT-ligated site, which is 10.8 and 7.0 kcal/mol smaller in magnitude than its QC counterparts with the aug-cc-pVTZ(-f) and cc-pVTZ(-f) bases, respectively.

It is to be noted that although they occur to a lesser degree, there also occur mutual compensations of trends between the energy contributions computed with the aug-cc-pVTZ and cc-pVTZ basis sets. Thus, for the ligated His_3 site (Table 6), ΔE(QC/aug-cc-pVTZ) is by only 2 kcal/mol out of 500 smaller than ΔE(QC/cc-pVTZ), yet E_1 and E_2 are by 8.7 and 6.5 kcal/mol smaller and larger in magnitude, respectively. In the ligated Asp-His_2 site (Table 7), ΔE(QC/aug-cc-pVTZ is 4.2 kcal/mol out of 580 smaller than ΔE(QC/cc-pVTZ), while E_1 and E_2 are correspondingly by 13.6 and 9.5 kcal/mol smaller and larger in magnitude.

Figure 9 illustrates the compared evolutions of ΔE(SIBFA) and ΔE(QC) and their contributions in the six complexes. With the exception of E_{ct}, the trends of the individual QC contributions are closely accounted for by their SIBFA counterparts, and the curves are very close. This is noteworthy, considering the amplitudes of the net charges of the complexes, which range from 3 to zero: +3 in complex B (dizinc site), +2 in complexes A (TZT−dizinc) and D (His_3 monozinc site), +1 in complexes C (TZT−His_3 monozinc) and F (Asp-His_2 monozinc site), and zero in complex E (TZT−Asp-His_2 monozinc site).

The present results also indicate that further refinements to SIBFA could be brought by seeking to improve E_{MTP*}. Thus, it was shown by Stone that with extended basis sets, the GDMA procedure can have shortcomings in the case of conjugated molecules, and that the quality of the multipolar representation can be very much dependent upon some parameters, such as the effective H radii used in the input.[36] The Iterative Stockholder (ISA)[47,48] and GEM[49,50] approaches are newly emerging alternatives to GDMA, less impacted by conjugation, and we plan to implement and evaluate these in forthcoming work.

3. Transferability. An essential issue at the outcome of these evaluations relates to transferability. Two aspects need to be considered: (a) Could the present TZT calibration be extended to all Zn−metalloprotein ligands embodying TZT as a zinc-binding motif? (b) Could such a calibration be applied "as is" to TZT derivatives differing from the present ligand by replacement of its amino group by another one, and/or by addition of a substituent to the ring?

(a) It is recalled that it is the essence of the SIBFA procedure to assemble a larger, flexible molecule, whether a macromolecule or a flexible ligand, upon resorting to the multipoles and polarizabilities of its individual fragments. This raises the issue of multipole transferability,[51] namely, following such an assembly as well as upon conformation changes, the multipoles can undergo significant changes in their intensities. Earlier on, we put forth a procedure addressing this issue and aiming to compute simultaneously and consistently both *intra*- and *inter*-molecular polarization and charge-transfer. It enabled to closely account for the QC results concerning conformational dependences of Zn-binding of glycine and the glycine zwitterions,[52] mercaptocarboxamides,[53] triphosphate[54] and, more recently, conformation-dependent solvation energies in a 64-water shell of four hydroxamate containing phosphomannose isomerase inhibitors.[20] Along these lines, a series of TZT-containing inhibitors, designed and tested in one of our Laboratories, has been assembled and their complexes with the VIM-2 MBL are presently optimized.[67]

(b) We have extended the present tests to two other TZT ligands. The first has a $-CH_3$ substituent replacing the amino one, and the second has in addition a $-CF_3$ substituent *ortho* to the $-CH_3$ group. We will thereafter denote by I, II and III the $-NH_2$, $-CH_3$, and $-CH_3-CF_3$ derivatives, respectively (see Figure 10). We have also considered another MBL binding site, that of the VIM-2 involved in nosocomial diseases. We have resorted to the X-ray structure of VIM-2 (compound TZT−CH_3−CF_3 is the one present in the crystallographic structure

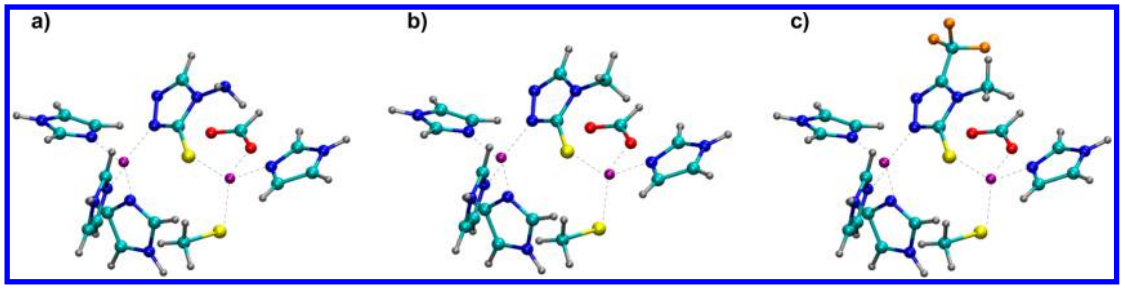

Figure 10. Active site of VIM-2 protein with (a) TZT, (b) TZT−CH_3, and (c) TZT−CH_3−CF_3 (N, blue; C, cyan; S, yellow; H, gray; Zn(II), purple; O, red; F, orange).

DOI: 10.1021/acs.jpcb.7b01053
J. Phys. Chem. B 2017, 121, 6295−6312

Table 8. Interaction Energies (kcal/mol) for VIM-2 without ligand

	dizinc site			$(His)_3$ site			(Asp-His-Cys) site		
	RVS			RVS			RVS		
energy contribution RVS/SIBFA	cc[a]	augcc[b]	SIBFA	cc	augcc	SIBFA	cc	augcc	SIBFA
E_C/E_{MTP*}	−860.8	NC[d]	−832.2	−294.7	−299.2	−281.4	−554.2	−551.4	−534.6
E_X/E_{REP}	251.3		258.3	136.4	144.7	138.1	100.8	109.4	103.2
E_{CX}/E_1	−609.5		−573.9	−158.3	−154.5	−143.3	−454.3	−442.0	−431.5
E_{POL}	−268.7		−309.7	−148.5	−159.0	−161.2	−89.4	−109.2	−109.0
$E_{POL(VAR)}$	−205.3		−254.2	−121.7	−131.2	−126.9	−75.7	−91.3	−99.6
E_{CT}	−121.1			−46.0	−38.4		−58.0	−44.5	
$E_{CT\text{-}BSSE}$	−112.2		−66.1	−44.0	−37.6	−31.7	−53.0	−44.2	−36.6
$E_{CT(Zn)}$	−1.7			−1.1	−0.9		−0.6	−0.6	
E_2	−317.5		−320.3	−165.7	−168.8	−163.8	−128.7	−135.5	−136.2
$\Delta E_{RVS}/\Delta E_{SIBFA}$[c]	**-927.6**		**−894.2**	**−324.0**	**−323.3**	**−307.1**	**−582.0**	**−577.5**	**−567.7**
ΔE_{HF}	**-935.9**			**−325.9**	**−324.1**		**−587.0**	**−577.8**	

[a]cc: cc-pVTZ(-f) basis set. [b]augcc: augcc-pVTZ(-f) basis set. [c]ΔE_{RVS} includes the BSSE correction [d]NC: non converged RVS

Table 9. Interaction Energies (kcal/mol) for VIM-2 with TZT Ligand

	dizinc site			$(His)_3$ site			(Asp-His-Cys) site		
	RVS			RVS			RVS		
energy contribution RVS/SIBFA	cc[a]	augcc[b]	SIBFA	cc	augcc	SIBFA	cc	augcc	SIBFA
E_C/E_{MTP*}	−1239.0	NC[d]	−1227.1	−554.0	−560.0	−550.9	−673.0	−675.5	−660.0
E_X/E_{REP}	430.4		431.9	201.0	215.8	204.9	218.0	237.6	209.9
E_{CX}/E_1	−808.6		−795.2	−353.0	−344.3	−346.0	−455.0	−437.9	−450.1
E_{POL}	−267.6		−300.8	−157.8	−170.9	−171.7	−108.7	−129.3	−122.8
$E_{POL(VAR)}$	−210.2		−225.0	−122.5	−132.8	−125.5	−89.9	−103.1	−97.3
E_{CT}	−109.3			−47.8	−41.7		−59.5	−52.1	
$E_{CT\text{-}BSSE}$	−97.7		−74.3	−44.1	−40.3	−33.3	−52.6	−51.2	−41.8
$E_{CT(Zn)}$	−3.7			−1.7	−1.6		−1.8	−1.6	
E_2	−307.9		−299.3	−166.6	−173.1	−160.1	−142.6	−154.3	−139.1
$\Delta E_{RVS}/\Delta E_{SIBFA}$[c]	**−1116.5**		**−1094.5**	**−519.6**	**−517.4**	**−506.1**	**−597.6**	**−592.2**	**−589.2**
ΔE_{HF}	**−1128.0**	**−1113.0**		**−523.3**	**−518.6**		**−604.5**	**−593.0**	

[a]cc: cc-pVTZ(-f) basis set. [b]augcc: augcc-pVTZ(-f) basis set. [c]ΔE_{RVS} includes the BSSE correction [d]NC: non converged RVS

Table 10. Interaction Energies (kcal/mol) for VIM-2 with TZT−CH_3 Ligand

	dizinc site			$(His)_3$ site			(Asp-His-Cys) site		
	RVS			RVS			RVS		
energy contribution RVS/SIBFA	cc[a]	augcc[b]	SIBFA	cc	augcc	SIBFA	cc	augcc	SIBFA
E_C/E_{MTP*}	−1249.7	NC[d]	−1239.7	−561.1	−567.5	−557.0	−676.6	−679.2	−666.6
E_X/E_{REP}	435.6		437.3	206.0	221.0	210.4	218.3	238.0	209.9
E_{CX}/E_1	−814.1		−802.4	−355.1	−346.5	−346.6	−458.4	−441.2	−456.7
E_{POL}	−266.2		−309.4	−158.5	−171.5	−180.2	−107.1	−127.5	−124.9
$E_{POL(VAR)}$	−209.6		−225.5	−123.4	−133.6	−132.9	−89.1	−102.1	−94.2
E_{CT}	−108.7			−48.1	−42.0		−58.8	−51.6	
$E_{CT\text{-}BSSE}$	−97.2		−72.4	−44.3	−40.6	−33.0	−51.9	−50.8	−40.3
$E_{CT(Zn)}$	−3.8			−1.8	−1.5		−1.8	−1.6	
E_2	−306.9		−297.9	−167.7	−174.2	−165.9	−141.0	−152.8	−134.6
$\Delta E_{RVS}/\Delta E_{SIBFA}$[c]	**−1120.9**		**−1100.3**	**−522.8**	**−520.7**	**−512.5**	**−599.4**	**−594.0**	**−591.3**
ΔE_{HF}	**−1132.4**	**−1117.5**		**−526.5**	**−522.1**		**−606.3**	**−594.9**	

[a]cc: cc-pVTZ(-f) basis set. [b]augcc: augcc-pVTZ(-f) basis set. [c]ΔE_{RVS} includes the BSSE correction [d]NC: non converged RVS

5ACW).[24] In the first zinc-binding site, Zn(II) is bound by three MBL residues (His) and the nitrogen atom ortho to the sulfur atom of the ligand. The second Zn(II) is coordinated by one Cys, one Asp, and one His residues and TZT through its S atom. For the purpose of the present evaluations, all three TZT ligands were set in the same geometry and single-point comparison with QC were done for it. The results are reported in Tables 8-11 regarding the dizinc site, and each zinc-biding site separately. Table 8 relates to the unligated MBL sites, and Tables 9−11 relate to their complexes with ligands I−III, respectively. The three complexes are presented in Figure 10a−c.

In the dizinc site, ΔE(SIBFA) has a distinct preference along the sequence II > I > III, ΔE(SIBFA) amounting to −1100.3, −1094.5, and −1088.8 kcal/mol, respectively. Taking I as

DOI: 10.1021/acs.jpcb.7b01053
J. Phys. Chem. B 2017, 121, 6295−6312

Table 11. Interaction Energies (kcal/mol) for VIM-2 with TZT−CH_3-CF_3 Ligand

	dizinc site			$(His)_3$ site			(Asp-His-Cys) site		
	RVS			RVS			RVS		
energy contribution RVS/SIBFA	cc[a]	augcc[b]	SIBFA	cc	augcc	SIBFA	cc	augcc	SIBFA
E_C/E_{MTP*}	NC[d]	NC	−1226.6	NC	−556.4	−549.0	NC	−675.1	−661.5
E_X/E_{REP}			444.4		224.8	216.6		235.9	210.8
E_{CX}/E_1			−782.3		−331.6	−332.4		−439.2	−450.7
E_{POL}			−322.6		−176.0	−184.9		−129.2	−131.2
$E_{POL(VAR)}$			−233.2		−137.0	−135.3		−102.8	−96.4
E_{CT}					−42.3			−51.9	
$E_{CT-BSSE}$			−73.2		−40.8	−33.7		−51.1	−40.8
$E_{CT(Zn)}$					−1.6			−1.6	
E_2			−306.5		−177.8	−169.1		−153.9	−137.2
$\Delta E_{RVS}/\Delta E_{SIBFA}$[c]			**−1088.8**		**−509.3**	**−501.4**		**−593.0**	**−587.9**
ΔE_{HF}	**−1120.6**	**−1106.9**		**−514.6**	**−510.5**		**−604.4**	**−593.9**	

[a]cc: cc-pVTZ(-f) basis set. [b]augcc: augcc-pVTZ(-f) basis set. [c]ΔE_{RVS} includes the BSSE correction [d]NC: non converged RVS.

the zero-energy, the relative difference are thus −5.8, 0, and +5.7 kcal/mol. These are significant differences in absolute values, but they are small in relative values, as they represent less than 1% of ΔE. How well do these results compare to the QC ones? While the augcc−pVTZ and cc-pVTZ results differ among themselves by a stable amount of 15 kcal/mol, they fully support the SIBFA results. Thus, ΔE (HF-augcc-pVTZ) amounts to −1117.5, −1113.0, and −1106.9 kcal/mol, resulting in −4.5, 0.0, and +6.1 kcal/mol differences. The energy agreements are also valid regarding the trends of the energy contributions. Thus, upon passing from I to II, E_1 has increased in magnitude by 5.5 and 7 kcal/mol in QC and SIBFA respectively. Such changes are due to large increases of E_{MTP*} and E_C partly compensated by corresponding increases of E_X/E_{rep}. The evolutions of E_{pol} and E_{ct} are significantly smaller. A different situation is observed when passing from II to III, namely, adding an ortho electron-withdrawing substituent. Now SIBFA results in 13 kcal/mol decrease of E_{MTP*} along with an increase of 7 kcal/mol of E_{rep}. There is thus a 20 kcal/mol drop of the E_1 value. On the other hand, E_2 (E_{pol} and E_{ct}) has increased in magnitude by 8.6 kcal/mol, as a reflection of the greater polarizability of the entirety of the TZT ring in III conferred by its − CF_3 substituent. We were not able to converge the RVS results for complex III in the dizinc site to support the present analyses, but the outcome in terms of overall ΔE, namely a difference of 10.6 kcal/mol in favor of II, close to the 11.5 kcal/mol SIBFA difference, should lend support to this analysis. Also, the trends of the SIBFA contributions for III versus II in the two separate monozinc sites are fully consistent with their aug-cc-pVTZ RVS counterparts, particularly for the most sensitive His_3 site. It is indeed very instructive to consider the trends in the individual Zn-binding sites. The energy ordering appears to be predominantly due to the His_3 site, even though this site is farther from the substituents, being "para" to them. The comparison of the two extreme complexes, namely II and III, shows clearly the impact of substitution by electron-donors or acceptors on both QC-derived distributed multipoles and polarizabilities. This observation reemphasizes the conclusions from a recent study.[55]

Another instructive finding relates to the distinct, separate trends of E_{pol} and E_{ct} in the two monozinc binding sites. Thus, considering the complexes of I, E_{pol} is favored in the His_3 site over the Asp-His-Cys site by a significant amount, 28.2 and 32.6 kcal/mol in SIBFA and QC, respectively, even though the imidazole ligands are neutral and less polarizable than the formate and methanethiolate ones. This is a clear indication of the lesser screening and nonadditivities taking place in such a site. By contrast, E_{ct} is favored in the Asp-His-Cys site by 8.5 and 8.5−10.9 kcal/mol in the SIBFA and QC calculations, respectively. This is due to the greater electron-donating properties of the cysteinate and formate ligands overcoming the much more unfavorable anticooperativities of E_{ct} than E_{pol} in ionic sites.[11]

4. Toward Inclusion of Correlation/Dispersion. The next step forward is inclusion of correlation/dispersion and comparisons to correlated QC calculations. In the most direct procedure, a dispersion contribution, E_{disp}, is added to ΔE and ΔE_{tot} is compared to ΔE(DFT-D3) in multimolecular complexes. This was evaluated recently upon studying the complexes of hydroxamate-based inhibitors with a Zn-metalloenzyme recognition site and discrete water molecules, totaling up to 265 atoms.[20] Even though small ΔE_{tot}(SIBFA) relative errors were reported (<3%), there are expectable improvements upon resorting to correlated multipoles and polarizabilities. This should enable for an improved control of nonadditivity (δE_{nadd}) in multimolecular complexes, particularly polyligated Zn(II) complexes. We adopt a staged approach. After the initial calibration and validation by EDA analyses at the HF level, we resort to distributed multipoles and polarizabilities from correlated B3LYP calculations on the fragments instead of the HF ones. This staged approach was recently followed upon studying the stacked and H-bonded complexes of cytosine dimers[56] and the channeling through two stacked guanine tetramers of one and two alkali cations.[57] No recalibration of the SIBFA parameters was found necessary for such complexes to reliably reproduce ΔE(DFT-B97D3) calculations at the outcome of the preliminary EDA HF validations. In the present study, we resort to EDA from SAPT calculations to recalibrate the Zn-parameters for E_{disp}. The results presented below are part of a wider-scope effort, in which the entire library of SIBFA fragments is being reconstructed with distributed multipoles from alternatives to the GDMA approach [Naseem-Khan et al, work in progress]. For the present purpose, we resort to the same B3LYP-correlated multipoles and polarizabilities for imidazole and formate as in ref 58. SAPT calculations were performed on the monoligated complexes of Zn(II) with water, formate, formamide, imidazole and methanethiolate. Detailed results will be presented in a forthcoming paper. At this stage

DOI: 10.1021/acs.jpcb.7b01053
J. Phys. Chem. B 2017, 121, 6295−6312

Table 12. Complexes of TZT with Zn(II) bound to S9 and N6. Comparison between SAPT, SIBFA, ALMOEDA and B97-D3 calculations. Single-point computations are reported at the SIBFA equilibrium distances. Energies in kcal/mol

	Zn(II) − S9 (d = 2.10 Å)				Zn(II) − N6 (d = 1.80 Å)			
energy contribution	SAPT	SIBFA	ALMOEDA	B97-D3	SAPT	SIBFA	ALMOEDA	B97-D3
E_C	−293.0	−296.0			−343.3	−334.5		
E_X	109.9	108.2			112.6	125.2		
E_1	−183.2	−187.8	−195.9		−230.8	−209.3	−235.6	
E_{ind}	−150.3	−156.8	−180.4		−126.7	−150.9	−160.1	
E_{disp}	−8.8	−8.5			−6.5	−11.1		
ΔE	−342.4	−356.1	−376.3	−376.6	−363.9	−371.3	−395.7	−410.3

we note that no recalibration of the ligand-specific parameters was found necessary for these ligands. On the basis of SAPT calculations of these complexes, we only had to modify the atom-type dependent pairwise multiplicative constants L_{Zn}-L of E_{disp}[12] which for L = N, O, and S now take the values 3.6, 4.7, and 3.0, respectively. The effective Zn(II) radius used to compute the penetration component of E_{MTP}* involving this cation was increased from 0.975[45] to 1.285 Å. We next derived correlated multipoles and polarizabilities for TZT. We report in Tables 12-13 comparisons between ΔE_{tot}(SIBFA) and its

Table 13. Complexes of TZT with H_2O bound to S9 and N6. Comparison between SAPT, and SIBFA calculations. Single-point computations are reported at the SIBFA equilibrium distances. Energies in kcal/mol

	H_2O − S9 (d = 2.40 Å)		H_2O − N6 (d = 2.00 Å)	
energy contribution	SAPT	SIBFA	SAPT	SIBFA
E_C	−13.4	−17.2	−14.1	−17.7
E_X	10.7	12.2	10.5	12.2
E_1	−2.7	−5.0	−3.6	−5.5
E_{ind}	−4.1	−2.1	−5.0	−4.8
E_{disp}	−3.1	−1.9	−3.1	−2.2
ΔE	−10.2	−10.2	−11.6	−12.4

contributions and SAPT-DFT, ALMOEDA, and B97-D3 calculations in the four in-plane complexes which enabled to recalibrate the TZT parameters: these are, respectively, those of Zn(II) bound to S9 or N6 in the same positions as in Tables 1 and 3, and of water donating a proton to either atom in the same orientations, the S/N, H, and O atoms being aligned. Only the values at the SIBFA equilibrium distances are given, the SAPT ones being the same or differing by only 0.1 Å. It has to be mentioned, however, that the correlated GDMA multipoles of TZT gave rise to much poorer agreements with E_C(SAPT) than the HF ones, despite our testing several effective hydrogen van der Waals radii, ranging from 0.10 to 0.40 in this context. This is an unsolved issue. Until alternatives to GDMA are implemented and tested, and for the present preliminary evaluations, we chose to retain the original TZT HF multipoles. With respect to the original parameters, the only changes brought bore on the increments of van der Waals increment of the sp^3 S9 and sp N6 lone-pairs: + 0.15 for S9 instead of −0.15, and 0. instead of −0.3 for N6. These translate expansions of the lone-pairs of an ionic, conjugated ring that occur due to correlation. Tables 12-13 show that the present calibration enables a satisfactory reproduction of ΔE(SAPT) in all four complexes, even though the numerical values of ΔE vary from −340 kcal/mol in the Zn(II) complexes, to −10 in the water complexes. For the two Zn complexes, even the correlated QC results can differ by large amounts between themselves: by up to 50 kcal/mol upon comparing SAPT and B97-D3. Nevertheless all methods provide similar preferences favoring N6 over S9 binding, namely by 21.5, 19.6, 15.7 kcal/mol for SAPT, ALMOEDA and B97-D3 respectively. The corresponding SIBFA difference is 15.2 kcal/mol. The present results will serve as a basis for subsequent refinements along with the use of ISA or GEM multipoles in a broader context.

We now seek to address the following point: upon reconsidering the L1 sites and their complexes, and pending ongoing refinements, could improved agreements with ΔE(B97-D3) be brought by the correlated multipoles and polarizabilities? The results are reported in Table 14. For the dizinc and the two monozinc sites and their complexes with TZT, it lists the ΔE(B97-D3) values with the cc-pVTZ and aug-cc-pVTZ basis sets along with the gain with respect to ΔE(HF) brought by correlation/dispersion. It then lists the ΔE(SIBFA) values, first with the uncorrelated multipoles and polarizabilities as in Tables 5-7 and then with their correlated counterparts. To ΔE are added the E_{disp} contributions with the appropriate calibration. We did not list the ΔE(MP2) results which were found to be very close in magnitude to the ΔE(B97-D3) results.

For all three unligated complexes, denoted as B, D, and F, the "uncorrelated" ΔE_{tot}(SIBFA) values are very close to ΔE(B97-D3) results, with relative errors <2%. A much lesser agreement occurs, however, with the ligated complexes. Thus, for the ligated dizinc complex A, the relative error can rise to up to and 4 and 5% with respect to the cc-pVTZ and aug-cc-pVTZ calculations, respectively. This indicates that complexes of soft divalent cations with anionic and conjugated ligands could be particularly sensitive to correlation and its impact, through E_{pol} and E_{ct}, on nonadditivity. Even though the present SIBFA correlated calculations have not yet reached a definite state of development, is there a hint toward an improved outcome? Regarding first the three unligated complexes B, D, and F, we can observe a slight reduction of the magnitude of ΔE_{tot} values as compared to their uncorrelated counterparts. It can reach 2% for complex A, but is not deemed to alter significantly the agreement with ΔE(B97-D3). A significant improvement of the agreement with ΔE(B97-D3) takes place, by contrast, in all three ligated complexes A, C, and E. For the two monozinc sites, ΔE_{tot}(SIBFA) now has very close values to ΔE(B97-D3) and in fact intermediate between the cc-pVTZ and aug-cc-pVTZ basis sets. The agreement is the clearest in complex A, where the relative error has been brought down from 5 to <2% regarding the aug-cc-pVTZ calculations and from 4 to 0.5% regarding the cc-pVTZ calculations.

With this approach it is also possible to unravel within E_{disp}(SIBFA) the contribution of correlation and that of the actual "van der Waals" term. The first, E_{corr}(SIBFA), is obtained as the difference between ΔE(SIBFA) computed with correlated and with uncorrelated multipoles and polarizabilities.

DOI: 10.1021/acs.jpcb.7b01053
J. Phys. Chem. B 2017, 121, 6295−6312

Table 14. L1 with TZT ring. Comparison between ΔE(QC/B97-D3) with the augcc-pVTZ(-f) and ccpvtz(-f) basis sets and ΔE_{tot}(SIBFA). For the latter, the results with both uncorrelated and correlated multipoles and polarizabilities are listed. The latter results list in parentheses the separate contributions to E_{disp}/corr of 'correlation' and dispersion. Energies in kcal/mol

		B97-D3		SIBFA	
complex	energy contribution	cc[a]	augcc[b]	uncorrelated multipoles and polarizabilities	correlated multipoles and polarizabilities
TZT−dizinc site ligated (*A*)	ΔE	−1001.2		−1103.8	−1034.0
	corr./disp.	−111.3		−147.9	−81.3 (−30.2,−51.1)
	ΔE_{tot}	**−1112.5**		**−1151.7**	**−1115.3**
unligated site (*B*)	ΔE	−724.4	−717.4	−707.6	−734.6
	corr./disp.	−93.0	−86.5	−92.9	−51.1 (−27.0,−24.1)
	ΔE_{tot}	**−817.4**	**−803.9**	**−800.5**	**−785.7**
TZT−$(His)_3$ site ligated (*C*)	ΔE	−512.9	−508.7	−509.9	−530.4
	corr./disp.	−52.4	−49.3	−65.4	−35.0 (−20.5, −14.5)
	ΔE_{tot}	**−565.3**	**−558.0**	**−575.3**	**−565.4**
unligated (*D*)	ΔE	−316.9	−315.4	−307.8	−323.2
	corr./disp.	−42.5	−40.9	−40.5	−21.4 (−15.4, −6.0)
	ΔE_{tot}	**−359.4**	**−356.3**	**−348.3**	**−344.6**
TZT−Asp-$(His)_2$ site ligated (*E*)	ΔE	−594.3	−586.0	−586.7	−603.0
	corr./disp.	−56.0	−50.8	−77.4	−42.7 (−16.3, −26.4)
	ΔE_{tot}	**−650.3**	**−636.8**	**−664.1**	**−645.7**
unligated(*F*)	ΔE	−487.0	−481.5	−473.0	−486.1
	corr./disp.	−41.3	−36.8	−47.4	−26.1 (−13.1, −13.0)
	ΔE_{tot}	**−528.3**	**−518.3**	**−520.4**	**−512.2**

[a]cc: cc-pVTZ(-f) basis set. [b]augcc: augcc-pVTZ(-f) basis set.

The second, E_{vdW}(SIBFA). is obtained as the difference between E_{disp} and E_{corr}. There is to our knowledge, no precedent to such decomposition. The values are given in parentheses. The values are well balanced, except in the case of the unligated His_3 site in which E_{vdW}(SIBFA) is less than half E_{corr}(SIBFA). TZT complexation favors more E_{vdW} than E_{corr}, owing to anticooperativity enhanced in its presence, which impacts E_{pol} and E_{ct}, whence E_{corr}.

CONCLUSIONS AND PERSPECTIVES

We have performed parallel QC and SIBFA computations to probe the in- and out-of-plane interaction modes of Zn(II) with a Zn(II)-binding ligand, 1,2,4-triazole-3-thione (TZT) which could be very promising in the search for novel MBL inhibitors to fight the bacterial resistance to antibiotics.[6,13] We have explored in detail Zn(II) binding to S9, and to its *ortho* nitrogen, N6, each of which takes part to the chelation of one Zn(II) in the dizinc sites of L1.[6] This chelation anchors TZT-based inhibitors in the MBL recognition site. Additional fragments grafted on TZT could contribute ionic, polar or π-stacking interactions with residues of the binding site. The in-register ligand−receptor fit can be very sensitive to the optimized structure of the anchoring TZT−dizinc complex. Overestimation of the Zn−S9 or Zn−N6 distances could lead to steric, instead of attractive, interactions of the TZT-connected groups with the targeted MBL residues. Conversely, underestimations of such distances could lead to suboptimal interactions with these residues. Improperly optimized θ and ϕ angles could in all cases be detrimental to such interactions. Furthermore, there are some target MBL's, such as NDM-1 for which no complex with TZT derivatives has been crystallized to date. This makes it all the more necessary to be able to account for the fine details of TZT−dizinc complexes prior to large-scale simulations of diverse TZT-based inhibitor-MBL complexes. The calibration of the TZT relevant parameters was performed on a limited subset of its Zn complexes, namely in-plane and perpendicular radial approaches to S9 and N6. The subsequent in- and out-of-plane angular variations showed that ΔE(SIBFA) closely matches ΔE(QC) in the energy-relevant zones, and has its angular minima at the same θ and ϕ values. Such agreements were also generally found between individual SIBFA and QC contributions, but there were some cases of mutually compensating errors, such as between short-range repulsion and charge transfer upon performing out-of-plane variations of S9-bound Zn(II) (see Figure 6).

The most stringent tests for transferability bore on the polyligated Zn(II) complexes of the MBL dizinc site. We focused first on L1, in which one zinc cation (Zn1) is coordinated by three His and nitrogen N6 of TZT, and the second zinc cation (Zn2) by two His, one Asp, and S9 of the ligand. The most critical complex is clearly the TZT−dizinc site complex in its entirety. But it was necessary to also evaluate how well the agreements between ΔE(SIBFA) and ΔE(QC) and their individual contributions would carry out in the unligated complex as well as in the two separate Zn(II) sites, whether ligated or unligated. We have thus considered six distinct complexes, having net charges ranging from zero to three. Very close agreements between ΔE(SIBFA) and ΔE(QC) were obtained, with relative errors <2%. The individual SIBFA contributions followed the trends of their QC counterparts upon passing from complex A (TZT-ligated dizinc site) to complex *F* (unligated Asp-His_2 site). The relative E_2/E_1 weights were closely accounted for as well in SIBFA, ranging from about one-third in the complex of TZT with the Asp-His_2 site (complex D) having a net null charge, to about one in the His_3 site, which has a net charge of +2. Two shortcomings were found at this stage, but they were mutually compensatory, and thus of limited impact. The first concerned E_{MTP*}, and the second concerned E_{ct}(SIBFA). These were discussed above, along with perspectives for improvement. It has to be noted that the close agreements between E_{rep}(SIBFA) and E_X(QC) have to a large extent benefitted from recent refinements in the

DOI: 10.1021/acs.jpcb.7b01053
J. Phys. Chem. B 2017, 121, 6295−6312

representations of conjugated sp and sp^2 lone-pairs "smearing" them partly on both sides of the lone-pair bearer plane.[45] Such refinements enabled to prevent underestimations of E_{rep} whenever the conjugated imidazole, formate, or TZT rings were approached from above. This occurred for some ligating His nitrogens and their *ortho* carbons, which were approached by the acidic H of a CH bond of a neighboring His residue, but also, for one His residue of the Asp-His_2 site, by Zn(II).

A second test for transferability bore on two other TZT derivatives. The first has an electron-donating substituent, $-CH_3$, replacing the amino substituent. The second has in addition an electron-withdrawing group, $-CF_3$, *ortho* to the methyl. We have compared the intermolecular interaction energies of the three compounds in the recognition site of another MBL, VIM-2, in which an anionic cysteinate residue replaces one His side-chain in the Asp-His_2 site. In the dizinc site, ΔE(SIBFA) ranked the three derivatives along the order: TZT$-CH_3$ > TZT> TZT$-CH_3-CF_3$. The same ordering was found by ΔE(QC) with very close magnitudes of both the numerical values and the relative energy differences. The ranking was imposed by E_1, with up to 20 kcal/mol between the $-CH_3$ and the $-CH_3-CF_3$ derivatives, while E_2, most favorable for the latter, reduced this difference by 10 kcal/mol. These trends were seen with both SIBFA and QC calculations. This reemphasizes on the one hand the need for separability of ΔE into well-identified contributions. On the other hand, it shows, in line with,[55] that the QC-derived multipoles and polarizabilities can fully reflect the impact of chemical substitution on the molecular electron density, thus on E_{MTP*}, E_{pol}, and E_{ct}. Consideration of the VIM-2 site has also highlighted the fact that E_{pol} and E_{ct} can have differing preferences. Thus, E_{pol} had a larger magnitude in the His_3 site, owing to lesser screening of the field, while conversely E_{ct} had a larger magnitude in the Asp-His-Cys site, owing to the presence of strong electron-donating ligands. This example shows that it could be illusory to try and entangle these two contributions into a single "induction-like" term. In the present case, this would entail a severe imbalance that would disfavor the anionic site.

We have finally investigated the impact of distributed multipoles and polarizabilities, rather than the HF-derived ones, on the intermolecular interaction energies in the L1 binding site. ΔE_{tot} was then computed with a dispersion contribution rescaled in preliminary SAPT calculations. At the present stage of development, in the unligated dizinc site and in both two unligated monozinc sites, ΔE_{tot} had its value reduced by a small amount (<2%) with respect to ΔE_{tot} with HF-derived multipoles and the standard E_{disp} calibration. But a significant improvement took place upon TZT ligation, the relative errors with respect to ΔE(B97-D3) reduced to <2%. This occurs because of an improved control, with such multipoles and polarizabilities, of nonadditivity effects coming into play at the correlated level in the presence of a "soft" anionic and highly delocalized ligand such as TZT. In this context, it has also been possible to unravel within E_{disp}(SIBFA) the contribution of correlation; and that of its "van der Waals" component. Such an analysis despite its simplicity, does not seem to have been performed before.

Following the present calibration, a series of TZT-based inhibitors has been assembled using the SIBFA library of fragments constructed with aug-cc-pVTZ(-f) multipoles and polarizabilities. Their complexes with VIM-2 are being presently energy-minimized prior to molecular dynamics. Preliminary results indicate that the structures of the TZT-dizinc complexes do remain close to the starting experimental one, enabling multipronged interactions of other entities with MBL recognition sites. These results will be reported in due course.

The QC-grounded calibration of a single zinc-binding group (ZBG) thus enables the construction of a diverse series of Zn-metalloprotein inhibitors. Could, on the other hand, the present calibration and validation strategy be automated for the design of new ZBG motifs? One rate-limiting step relates to the QC EDA calculations needed to probe its relevant atoms, by performing radial as well as in- and out-of-plane angular variations. While such a step can be automated, its only limitation is in the lag time needed to process and execute the QC calculations.

Regarding the SIBFA calculations, the derivations of the multipoles and polarizabilities has to be done only once for any new ZBG fragments and is eased by automated procedures to derive these from the fragment MOs. Only a limited number of ligand-specific parameters then need to be calibrated, such as those used for the screening of the polarizing fields, to fine-tune the internal coordinates of the lone-pairs on the basis of ELF calculations[59−62] and the increments of the bearer radii along the lone-pair direction on the basis of the EDA results to match the radial dependencies of E_X(QC) and E_{ct}(QC). Such parameters can themselves be optimized by automated procedures such as INoLLS.[63,64] Thus, perspectives do exist toward fastened construction, calibration and validations of novel motifs, and the Lego-like assembly of a wide diversity of novel molecules.

We are presently extending the construction of the SIBFA library with correlated aug-cc-p-VTZ multipoles and polarizabilities. ΔE(SIBFA) and its contributions, now integrating correlation effects, as well as E_{disp}, are being recalibrated on the basis of SAPT EDA's. The present calibration of TZT will be used as a starting point for the ensuing one at the correlated level. Results obtained so far on several building-block fragments indicate that only a limited recalibration of the ligand-specific parameters could be necessary.

The SIBFA potential and its gradients have been integrated in a new version of the massively parallel Tinker-HP code.[65] It is destined to be released in the forthcoming year. This should enable potential users to validate and use it in a diversity of molecular recognition systems and ligand-macromolecule complexes.

The present benchmark calculations could be used by other force-field developers to test their own potentials. For that purpose, we give in Supporting Information the coordinates of all TZT-based dizinc complexes used in this paper (Tables S7−S10).

■ ASSOCIATED CONTENT

Supporting Information

The Supporting Information is available free of charge on the ACS Publications website at DOI: 10.1021/acs.jpcb.7b01053.

Representation of the lone pairs (in pink) of the TZT ring, comparisons between QM and SIBFA interaction energies and their contributions as a function of distance or angle for various geometries of approach of a Zn(II) or a water probe to S6 and N9 atoms, locations of the lone pairs in terms of internal coordinates, occupation numbers and effective radii increments, evolutions of the QC and SIBFA interaction energies and their contributions in various Zn(II) or water−TZT complexes, and coordinates of the dizinc complex of L1 with TZT, and

DOI: 10.1021/acs.jpcb.7b01053
J. Phys. Chem. B 2017, 121, 6295−6312

of VIM-2 with TZT, TZT−CH_3, and TZT−CH_3−CF_3 (PDF)

AUTHOR INFORMATION

Corresponding Author

*(N.G.) E-mail: gresh@lct.jussieu.fr.

ORCID

Jean-Philip Piquemal: 0000-0001-6615-9426

Nohad Gresh: 0000-0001-7174-2907

Notes

The authors declare no competing financial interest.

ACKNOWLEDGMENTS

The research by Karolina Kwapien, Mirna Damergi and Serge Nader was supported by a grant funded by the Agence Nationale de la Recherche (No. ANR-14-CE16-0028-01). We wish to thank the Grand Equipement National de Calcul Intensif (GENCI), Institut du Développement et des Ressources en Informatique Scientifique (IDRIS), Centre Informatique de l'Enseignement Supérieur (CINES, France, Project No. x2009-075009) and the Centre Régional Informatique et d'Applications Numériques de Normandie (CRIANN, Rouen, France, Project 1998053). L.E.K. sincerely thanks the Research Council of Saint-Joseph University of Beirut, Lebanon, the Lebanese National Council for Scientific Research, CNRS-L, as well as the French Institute-Campus France au Liban and the French−Lebanese program CEDRE for funding the Ph.D. thesis of L.E.K. and for their financial support to our researches. We also wish to thank the reviewers for constructive criticism.

REFERENCES

(1) Bebrone, C. Metallo-β-Lactamases (Classification, Activity, Genetic Organization, Structure, Zinc Coordination) and Their Superfamily. *Biochem. Pharmacol.* **2007**, *74*, 1686−1701.

(2) Palzkill, T. Metallo-β-Lactamase Structure and Function. *Ann. N. Y. Acad. Sci.* **2013**, *1277*, 91−104.

(3) Toleman, M. A.; Walsh, T. R. Reply to "Genetic Contexts of blaNDM-1". *Antimicrob. Agents Chemother.* **2012**, *56*, 6071.

(4) Nordmann, P. Carbapenemase-Producing Enterobacteriaceae: Overview of a Major Public Health Challenge. *Med. Mal. Infect.* **2014**, *44*, 51−56.

(5) Ullah, J. H.; Walsh, T. R.; Taylor, I. A.; Emery, D. C.; Verma, C. S.; Gamblin, S. J.; Spencer, J. The Crystal Structure of the L1Metallo-β-Lactamase from Stenotrophomonas maltophilia at 1.7 Å Resolution. *J. Mol. Biol.* **1998**, *284*, 125−136.

(6) Nauton, L.; Kahn, R.; Garau, G.; Hernandez, J.-F.; Dideberg, O. Structural Insights into the Design of Inhibitors for the L1Metallo-β-lactamase from Stenotrophomonas maltophilia. *J. Mol. Biol.* **2008**, *375*, 257−269.

(7) Garcia-Saez, I.; Docquier, J.-D.; Rossolini, G. M.; Dideberg, O. The Three-Dimensional Structure of VIM-2, a Zn-β-Lactamase from Pseudomonas aeruginosa in Its Reduced and Oxidised Form. *J. Mol. Biol.* **2008**, *375*, 604−611.

(8) Zhang, H.; Hao, Q. Crystal Structure of NDM-1 Reveals a Common β-Lactam Hydrolysis Mechanism. *FASEB J.* **2011**, *25*, 2574−2582.

(9) Walsh, T. R. Emerging Carbapenemases: a Global Perspective. *Int. J. Antimicrob. Agents* **2010**, *36*, S8−S14.

(10) Nordmann, P.; Naas, T.; Poirel, L. Global Spread of Carbapenemase-Producing Enterobacteriaceae. *Emerging Infect. Dis.* **2011**, *17*, 1791−1798.

(11) Tiraboschi, G.; Gresh, N.; Giessner-Prettre, C.; Pedersen, L. G.; Deerfield, D. W. Parallel Ab Initio and Molecular Mechanics Investigation of Polycoordinated Zn(II) Complexes with Model Hard and Soft Ligands: Variations of Binding Energy and of Its Components with Number and Charges of Ligands. *J. Comput. Chem.* **2000**, *21*, 1011−1039.

(12) Gresh, N.; Piquemal, J.-P.; Krauss, M. Representation of Zn(II) Complexes in Polarizable Molecular Mechanics. Further Refinements of the Electrostatic and Short-Range Contributions. Comparisons with Parallel Ab Initio Computations. *J. Comput. Chem.* **2005**, *26*, 1113−1130.

(13) Olsen, L.; Jost, S.; Adolph, H.-W.; Pettersson, I.; Hemmingsen, L.; Jørgensen, F. S. New Leads of Metallo-β-Lactamase Inhibitors from Structure-Based Pharmacophore Design. *Bioorg. Med. Chem.* **2006**, *14*, 2627−2635.

(14) Faridoon; Hussein, W. M.; Vella, P.; Islam, N. U.; Ollis, D. L.; Schenk, G.; McGeary, R. P. 3-Mercapto-1,2,4-Triazoles and N-Acylated Thiosemicarbazides as Metallo-β-Lactamase Inhibitors. *Bioorg. Med. Chem. Lett.* **2012**, *22*, 380−386.

(15) Feng, L.; Yang, K.-W.; Zhou, L.-S.; Xiao, J.-M.; Yang, X.; Zhai, L.; Zhang, Y.-L.; Crowder, M. W. N-Heterocyclic Dicarboxylic Acids: Broad-Spectrum Inhibitors of Metallo-β-Lactamases with co-Antibacterial Effect Against Antibiotic-Resistant Bacteria. *Bioorg. Med. Chem. Lett.* **2012**, *22*, 5185−5189.

(16) Zhang, Y.-L.; Yang, K.-W.; Zhou, Y.-J.; LaCuran, A. E.; Oelschlaeger, P.; Crowder, M. W. Diaryl-Substituted Azolylthioacetamides: Inhibitor Discovery of New Delhi Metallo-β-Lactamase-1 (NDM-1). *ChemMedChem* **2014**, *9*, 2445−2448.

(17) Gresh, N.; Cisneros, G. A.; Darden, T. A.; Piquemal, J.-P. Anisotropic, Polarizable Molecular Mechanics Studies of Inter- and Intramolecular Interactions and Ligand-Macromolecule Complexes. A Bottom-Up Strategy. *J. Chem. Theory Comput.* **2007**, *3*, 1960−1986.

(18) Roux, C.; Gresh, N.; Perera, L. E.; Piquemal, J.-P.; Salmon, L. Binding of 5-Phospho-D-Arabinonohydroxamate and 5-Phospho-D-Arabinonate Inhibitors to Zinc Phosphomannose Isomerase from Candida Albicans Studied by Polarizable Molecular Mechanics and Quantum Mechanics. *J. Comput. Chem.* **2007**, *28*, 938−957.

(19) Gresh, N.; de Courcy, B.; Piquemal, J.-P.; Foret, J.; Courtiol-Legourd, S.; Salmon, L. Polarizable Water Networks in Ligand-Metalloprotein Recognition. Impact on the Relative Complexation Energies of Zn-Dependent Phosphomannose Isomerase with d-Mannose 6-Phosphate Surrogates. *J. Phys. Chem. B* **2011**, *115*, 8304−8316.

(20) Gresh, N.; Perahia, D.; de Courcy, B.; Foret, J.; Roux, C.; El Khoury, L.; Piquemal, J.-P.; Salmon, L. Complexes of a Zn-Metalloenzyme Binding Site with Hydroxamate-Containing Ligands. A Case for Detailed Benchmarkings of Polarizable Molecular Mechanics/Dynamics Potentials When the Experimental Binding Structure Is Unknown. *J. Comput. Chem.* **2016**, *37*, 2770−2782.

(21) Antony, J.; Gresh, N.; Olsen, L.; Hemmingsen, L.; Schofield, C. J.; Bauer, R. Binding of D- and L-captopril Inhibitors to Metallo-β-Lactamase Studied by Polarizable Molecular Mechanics and Quantum Mechanics. *J. Comput. Chem.* **2002**, *23*, 1281−1296.

(22) Antony, J.; Piquemal, J.-P.; Gresh, N. Complexes of Thiomandelate and Captopril Mercaptocarboxylate Inhibitors to Metallo-β-Lactamase by Polarizable Molecular Mechanics. Validation on Model Binding Sites by Quantum Chemistry. *J. Comput. Chem.* **2005**, *26*, 1131−1147.

(23) de Courcy, B.; Piquemal, J.-P.; Garbay, C.; Gresh, N. Polarizable Water Molecules in Ligand-Macromolecule Recognition. Impact on the Relative Affinities of Competing Pyrrolopyrimidine Inhibitors for FAK Kinase. *J. Am. Chem. Soc.* **2010**, *132*, 3312−3320.

(24) Christopeit, T.; Carlsen, T. J. O.; Helland, R.; Leiros, H.-K. S. Discovery of Novel Inhibitor Scaffolds against the Metallo-β-lactamase VIM-2 by Surface Plasmon Resonance (SPR) Based Fragment Screening. *J. Med. Chem.* **2015**, *58*, 8671−8682.

(25) Dunning, T. H. Gaussian Basis Sets for Use in Correlated Molecular Calculations. I. The Atoms Boron through Neon and Hydrogen. *J. Chem. Phys.* **1989**, *90*, 1007−1023.

(26) Feller, D. The Role of Databases in Support of Computational Chemistry Calculations. *J. Comput. Chem.* **1996**, *17*, 1571−1586.

DOI: 10.1021/acs.jpcb.7b01053
J. Phys. Chem. B 2017, 121, 6295−6312

(27) Stevens, W. J.; Fink, W. H. Frozen Fragment Reduced Variational Space Analysis of Hydrogen Bonding Interactions. Application to the Water Dimer. *Chem. Phys. Lett.* **1987**, *139*, 15−22.
(28) Schmidt, M. W.; Baldridge, K. K.; Boatz, J. A.; Elbert, S. T.; Gordon, M. S.; Jensen, J. H.; Koseki, S.; Matsunaga, N.; Nguyen, K. A.; Su, S.; et al. General Atomic and Molecular Electronic Structure System. *J. Comput. Chem.* **1993**, *14*, 1347−1363.
(29) Boys, S. F.; Bernardi, F. The Calculation of Small Molecular Interactions by the Differences of Separate Total Energies. Some Procedures With Reduced Errors. *Mol. Phys.* **1970**, *19*, 553−566.
(30) Grimme, S.; Antony, J.; Ehrlich, S.; Krieg, H. A Consistent and Accurate Ab Initio Parametrization of Density Functional Dispersion Correction (DFT-D) for the 94 Elements H-Pu. *J. Chem. Phys.* **2010**, *132*, 154104.
(31) Frisch, M. J.; Trucks, G. W.; Schlegel, H. B.; Scuseria, G. E.; Robb, M. A.; Cheeseman, J. R.; Scalmani, G.; Barone, V.; Mennucci, B.; Petersson, G. A.et al. *Gaussian 09*, Revision B.01; Wallingford, CT, 2009.
(32) Hohenstein, E. G.; Sherrill, C. D. Density Fitting of Intramonomer Correlation Effects in Symmetry-Adapted Perturbation Theory. *J. Chem. Phys.* **2010**, *133*, 014101.
(33) Turney, J. M.; Simmonett, A. C.; Parrish, R. M.; Hohenstein, E. G.; Evangelista, F.; Fermann, J. T.; Mintz, B. J.; Burns, L. A.; Wilke, J. J.; Abrams, M. L.; et al. Psi4: An Open-Source Ab Initio Electronic Structure Program. *WIREs Comput. Mol. Sci.* **2012**, *2*, 556−565.
(34) Khaliullin, R. Z.; Cobar, E. A.; Lochan, R. C.; Bell, A. T.; Head-Gordon, M. Unravelling the Origin of Intermolecular Interactions Using Absolutely Localized Molecular Orbitals. *J. Phys. Chem. A* **2007**, *111*, 8753−8765.
(35) Shao, Y.; Gan, Z.; Epifanovsky, E.; Gilbert, A. T. B.; Wormit, M.; Kussmann, J.; Lange, A. W.; Behn, A.; Deng, J.; Feng, X.; et al. Advances in Molecular Quantum Chemistry Contained in the Q-Chem 4 Program Package. *Mol. Phys.* **2015**, *113*, 184−215.
(36) Stone, A. J. Distributed Multipole Analysis: Stability for Large Basis Sets. *J. Chem. Theory Comput.* **2005**, *1*, 1128−1132.
(37) Stone, A. J. Electrostatic Damping Functions and the Penetration Energy. *J. Phys. Chem. A* **2011**, *115*, 7017−7027.
(38) Piquemal, J.-P.; Gresh, N.; Giessner-Prettre, C. Improved Formulas for the Calculation of the Electrostatic Contribution to the Intermolecular Interaction Energy from Multipolar Expansion of the Electronic Distribution. *J. Phys. Chem. A* **2003**, *107*, 10353−10359.
(39) Piquemal, J.-P.; Chevreau, H.; Gresh, N. Toward a Separate Reproduction of the Contributions to the Hartree-Fock and DFT Intermolecular Interaction Energies by Polarizable Molecular Mechanics with the SIBFA Potential. *J. Chem. Theory Comput.* **2007**, *3*, 824−837.
(40) Garmer, D. R.; Stevens, W. J. Transferability of Molecular Distributed Polarizabilities from a Simple Localized Orbital Based Method. *J. Phys. Chem.* **1989**, *93*, 8263−8270.
(41) Gresh, N. Model, Multiply Hydrogen-Bonded Water Oligomers (N = 3−20). How Closely Can a Separable, Ab Initio-Grounded Molecular Mechanics Procedure Reproduce the Results of Supermolecule Quantum Chemical Computations? *J. Phys. Chem. A* **1997**, *101*, 8680−8694.
(42) Creuzet, S.; Langlet, J.; Gresh, N. Adjustment of the SIBFA Method for Potential Maps to Study Hydrogen Bonding Vibrational Frequencies. *J. Chim. Phys. Phys.-Chim. Biol.* **1991**, *88*, 2399−2409.
(43) Dupuis, M.; Marquez, A.; Davidson, E. R. HONDO 95.3, QCPE, Bloomington, IN. Web site: https://t1.chem.umn.edu/hondoplus. Accessed 30 May 2017.
(44) Gresh, N. Energetics of Zn^{2+} Binding to a Series of Biologically Relevant Ligands: a Molecular Mechanics Investigation Grounded on Ab Initio Self-Consistent Field Supermolecular Computations. *J. Comput. Chem.* **1995**, *16*, 856−882.
(45) El Khoury, L.; Naseem-Khan, S.; Kwapien, K.; Perahia, D.; Hobaika, Z.; Maroun, R.; Piquemal, J.-P.; Gresh, N. Importance of explicit smeared lone-pairs in anisotropic polarizable molecular mechanics. Torture track angular tests for exchange-repulsion and charge transfer contributions. *J. Comput. Chem.* **2017**, DOI: 10.1002/jcc.24830.
(46) Gresh, N.; Garmer, D. R. Comparative Binding Energetics of Mg^{2+}, Ca^{2+}, Zn^{2+}, and Cd^{2+} to Biologically Relevant Ligands: Combined Ab Initio SCF Supermolecule and Molecular Mechanics Investigation. *J. Comput. Chem.* **1996**, *17*, 1481−1495.
(47) Misquitta, A. J.; Stone, A. J.; Fazeli, F. Distributed Multipoles from a Robust Basis-Space Implementation of the Iterated Stockholder Atoms Procedure. *J. Chem. Theory Comput.* **2014**, *10*, 5405−5418.
(48) Lillestolen, T. C.; Wheatley, R. J. Atomic Charge Densities Generated Using an Iterative Stockholder Procedure. *J. Chem. Phys.* **2009**, *131*, 144101.
(49) Elking, D. M.; Cisneros, G. A.; Piquemal, J.-P.; Darden, T. A.; Pedersen, L. G. Gaussian Multipole Model (GMM). *J. Chem. Theory Comput.* **2010**, *6*, 190−202.
(50) Cisneros, G. A. Application of Gaussian Electrostatic Model (GEM) Distributed Multipoles in the AMOEBA Force Field. *J. Chem. Theory Comput.* **2012**, *8*, 5072−5080.
(51) Faerman, C. H.; Price, S. L. A Transferable Distributed Mutlipole Model for the Electrostatic Interactions of Peptides and Amides. *J. Am. Chem. Soc.* **1990**, *112*, 4915−4626.
(52) Rogalewicz, F.; Ohanessian, G.; Gresh, N. Interaction of Neutral and Zwitterionic Glycine with Zn^{2+} in Gas Phase: Ab Initio and SIBFA Molecular Mechanics Calculations. *J. Comput. Chem.* **2000**, *21*, 963−973.
(53) Tiraboschi, G.; Fournie-Zaluski, M. C.; Roques, B. P.; Gresh, N. Intramolecular Chelation of Zn^{2+} by α- and β-Mercaptocarboxamides. A Parallel Ab Initio and Polarizable Molecular Mechanics Investigation. Assessment of the Role of Multipole Transferability. *J. Comput. Chem.* **2001**, *22*, 1038−1047.
(54) Gresh, N.; Shi, G. B. Conformation-Dependent Intermolecular Interaction Energies of the Triphosphate Anion with Divalent Metal Cations. Application to the ATP-Binding Site of Binuclear Bacterial Enzyme. A Parallel Quantum Chemical and Polarizable Molecular Mechanics Investigation. *J. Comput. Chem.* **2004**, *25*, 160−168.
(55) El Hage, K.; Piquemal, J.-P.; Hobaika, Z.; Maroun, R. G.; Gresh, N. Substituent-Modulated Affinities of Halobenzene Derivatives to the HIV-1 Integrase Recognition Site. Analyses of the Interaction Energies by Parallel Quantum Chemical and Polarizable Molecular Mechanics. *J. Phys. Chem. A* **2014**, *118*, 9772−9782.
(56) Gresh, N.; Sponer, J. E.; Devereux, M.; Gkionis, K.; de Courcy, B.; Piquemal, J.-P.; Sponer, J. Stacked and H-Bonded Cytosine Dimers. Analysis of the Intermolecular Interaction Energies by Parallel Quantum Chemistry and Polarizable Molecular Mechanics. *J. Phys. Chem. B* **2015**, *119*, 9477−9495.
(57) Gresh, N.; Naseem-Khan, S.; Lagardere, L.; Piquemal, J. P.; Sponer, J. E.; Sponer, J. Channeling through Two Stacked Guanine Quartets of One and Two Alkali Cations in the Li^+, Na^+, K^+ and Rb^+ Series. Assesment of the Accuracy of the SIBFA Anisotropic Polarizable Molecular Mechanics Potential. *J. Phys. Chem. B* **2017**, *121*, 3997.
(58) Dudev, T.; Devereux, M.; Meuwly, M.; Lim, C.; Piquemal, J. P.; Gresh, N. Quantum-Chemistry Based Calibration of the Alkali Metal Cations Series (Li^+-Cs^+) for Large-Scale Polarizable Molecular Mechanics/Dynamics Simulations. *J. Comput. Chem.* **2015**, *36*, 285−302.
(59) Becke, A. D.; Edgecombe, K. E. A Simple Measure of Electron Localization in Atomic and Molecular Systems. *J. Chem. Phys.* **1990**, *92*, 5397−5403.
(60) Silvi, B.; Savin, A. Classification of Chemical Bonds Based on Topological Analysis of Electron Localization Functions. *Nature* **1994**, *371*, 683−686.
(61) Chaudret, R.; Gresh, N.; Cisneros, G. A.; Scemama, A.; Piquemal, J.-P. Further Refinements of Next-Generation Force Fields - Nonempirical Localization of Off-Centered Points in Molecules. *Can. J. Chem.* **2013**, *91*, 804−810.
(62) Goldwaser, E.; de Courcy, B.; Demange, L.; Garbay, C.; Raynaud, F.; Hadj-Slimane, R.; Piquemal, J.-P.; Gresh, N. Conformational Analysis of a Polyconjugated Protein-Binding Ligand by Joint

DOI: 10.1021/acs.jpcb.7b01053
J. Phys. Chem. B 2017, 121, 6295−6312

Quantum Chemistry and Polarizable Molecular Mechanics. Addressing the Issues of Anisotropy, Conjugation, Polarization, and Multipole Transferability. *J. Mol. Model.* **2014**, *20*, 1−24.
(63) Law, M. M.; Hutson, J. M. I-NoLLS: A Program for Interactive Nonlinear Least-Squares Fitting of the Parameters of Physical Models. *Comput. Phys. Commun.* **1997**, *102*, 252−268.
(64) Devereux, M.; Gresh, N.; Piquemal, J.-P.; Meuwly, M. A Supervised Fitting Approach to Force Field Parametrization with Application to the SIBFA Polarizable Force Field. *J. Comput. Chem.* **2014**, *35*, 1577−1591.
(65) Tinker HP_Team, Tinker-HP, http://www.ip2ct.upmc.fr/tinkerHP, 2016 (accessed March 29, 2107).
(66) Piquemal, J. P.; Giessner-Prettre, C. Unpublished work.
(67) Kwapien et al. Work in progress

DOI: 10.1021/acs.jpcb.7b01053
J. Phys. Chem. B 2017, 121, 6295−6312